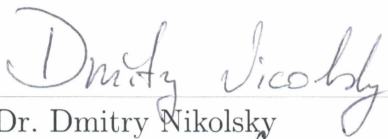


NUMERICAL REALIZATION OF THE GENERALIZED CARRIER-GREENSPAN
TRANSFORM FOR THE SHALLOW WATER WAVE EQUATIONS

By

Matthew W. Harris

RECOMMENDED:



Dr. Dmitry Nikolsky



Dr. Gordon Williams



Dr. Alexei Rybkin
Advisory Committee Chair

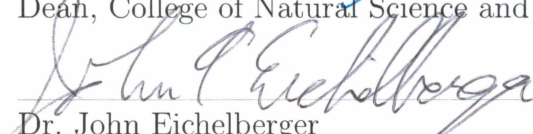


Dr. John Rhodes
Chair, Department of Mathematics and Statistics

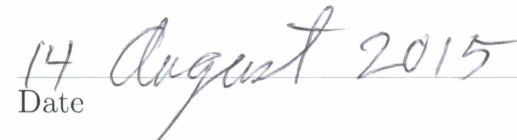
APPROVED:



Dr. Paul Layer
Dean, College of Natural Science and Mathematics



Dr. John Eichelberger
Dean of the Graduate School



Date

NUMERICAL REALIZATION OF THE GENERALIZED CARRIER-GREENSPAN
TRANSFORM FOR THE SHALLOW WATER WAVE EQUATIONS

A
THESIS

Presented to the Faculty
of the University of Alaska Fairbanks
in Partial Fulfillment of the Requirements
for the Degree of

MASTER OF SCIENCE

By
Matthew W. Harris, B.S.

Fairbanks, Alaska

August 2015

Abstract

We study the development of two numerical algorithms for long nonlinear wave runup that utilize the generalized Carrier-Greenspan transform. The Carrier-Greenspan transform is a hodograph transform that allows the Shallow Water Wave equations to be transformed into a linear second order wave equation with nonconstant coefficients. In both numerical algorithms the transform is numerically implemented, the resulting linear system is numerically solved and then the inverse transformation is implemented. The first method we develop is based on an implicit finite difference method and is applicable to constantly sloping bays of arbitrary cross-section. The resulting scheme is extremely fast and shows promise as a fast tsunami runup solver for wave runup in coastal fjords and narrow inlets. For the second scheme, we develop an initial value boundary problem corresponding to an inclined bay with U or V shaped cross-sections that has a wall some distance from the shore. A spectral method is applied to the resulting linear equation in order to find a series solution. Both methods are verified against an analytical solution in an inclined parabolic bay with positive results and the first scheme is compared to the 3D numerical solver FUNWAVE with positive results.

Table of Contents

	Page
Signature Page	i
Title Page	iii
Abstract	v
Table of Contents	vii
List of Figures	ix
List of Tables	xi
Acknowledgments	xiii
Chapter 1: Introduction	1
1.1 Chapter Overview	5
Chapter 2: Carrier-Greenspan Transform	7
2.1 Generalized Carrier-Greenspan Transformation	7
2.2 Computing $F(\sigma)$ for Bays of Interest	9
2.2.1 $F(\sigma)$ for U and V Shaped Bays	9
2.2.2 $F(\sigma)$ for a Trapezoidal Bay	10
2.3 Analytical Solution in a Parabolic Bay	11
2.4 Numerical Implementation of the Carrier-Greenspan Transformation	13
2.5 Conclusions	14
Chapter 3: Numerically Solving the SWEs in an Infinite Sloping Bay with Constant Cross-Sections	15
3.1 Numerical Algorithm for Runup in Bays of Infinite Length	15
3.1.1 Development of an Initial Value Boundary Problem (IVBP)	16
3.1.2 Numerical Algorithm	17

3.2	Verification and Validation of the Numerical Method	19
3.2.1	Verification in a Parabolic Bay	19
3.2.2	Validation in a Trapezoidal Bay	23
3.3	Conclusions	26
Chapter 4: Spectral Solution for U and V Shaped Bays of Finite Length . .		29
4.1	Development of an IVBP	29
4.2	Spectral Solution to the IVBP	31
4.3	Numerical Implementation of the Spectral Solution	33
4.4	Verification and Validation of the Spectral Method	34
4.4.1	Verification in a Parabolic Bay	34
4.5	Runup in U vs. V Shaped Bays	35
4.6	Conclusions	36
Chapter 5: Conclusions		39
References		41

List of Figures

	Page
<p>Figure 1.1 Top Left: a (x,z) cross-sectional view of an N-wave in a constantly sloping parabolic bay, Top Right: a (y,z) cross-sectional view of a parabolic bay with water displacement $\eta(x)$, and Bottom: the 3D view of the bay and N-wave given by the two cross-sections.</p>	4
<p>Figure 2.1 Top: A schematic view of a wave propagating in the trapezoidal beach with lateral walls slope $\beta = 1/2$, bottom width of $2y_0 = 100$ meters and the beach inclination of $\alpha = 0.01$. Bottom: a transverse cross-section of the bay.</p>	12
<p>Figure 2.2 Initial condition in physical coordinates for an analytical solution for the runup problem in a parabolic bay.</p>	13
<p>Figure 3.1 Top Left: the numerically computed wave dynamics in non-physical coordinates (σ, λ). The shoreline is fixed at $\sigma = 0$. Top Right: the numerically computed wave dynamics in physical coordinates (x, t). Bottom Left: the shoreline dynamics of the physical wave by restricting the x axis to $[-1.5, 20]$. The shoreline varies around $x = 0$. Bottom Right: the discrepancy between the analytical and numerical solution in the physical coordinates. The maximum errors occur at the runup (0.35%) and rundown (0.65%).</p>	21
<p>Figure 3.2 Left: loglog plot showing the errors given in Table 3.1, Right: loglog plot showing the errors given in Table 3.2</p>	22
<p>Figure 3.3 Relative error in the semianalytic method in a parabolic bay as a function of wave height. Note that the only factor that is changing in our semianalytic model is the initial wave height and that the error is always below .5% relative error. Furthermore the rate of change in the relative error decreases as the wave height increases.</p>	23

Figure 3.4	Schematic description of a submarine landslide. The landslide quickly moves material from its original location (A) to its resting location (B). This movement typically generates a N-wave.	25
Figure 3.5	Comparison of the water level computed by the semi-analytic and FUN-WAVE models.	27
Figure 4.1	Left: the accuracy in the approximation of the initial condition using our spectral method, Right: The coefficients in the spectral expansion corresponding to the initial condition to the left.	36
Figure 4.2	Top Left: the wave dynamics as computed by the spectral method. The black lines show a domain where our spectral solution can be compared against the analytic one. Top Right: analytic solution to be compared to our spectral method. Bottom: The relative error in terms of the maximum runup. The maximum errors occur at the runup (0.3%) and rundown (0.4%).	37
Figure 4.3	The effect of m on runup. Recall that bays with $0 < m \leq 1$ are V shaped bays and bays with $m > 1$ are the U shaped bays. This plot shows that for the initial condition, the runup in V shaped bays is significantly larger than the runup in U shaped bays.	38

List of Tables

		Page
Table 3.1	The relative error $\ R_u - \tilde{R}_u\ /R_u$ in the runup for different values of $\Delta\lambda$ and $\Delta\sigma$ values.	22
Table 3.2	The relative error $\ R_d - \tilde{R}_d\ /R_d$ in the rundown for different values of $\Delta\lambda$ and $\Delta\sigma$ values.	22
Table 3.3	Convergence of the \tilde{R}_u computed by the semi-analytical model. Note that the rundown in the FUNWAVE simulation is 0.9500 cm.	26
Table 3.4	Convergence of \tilde{R}_d computed by the semi-analytical model. Note that the rundown in the FUNWAVE simulation is -0.4069 cm.	26

Acknowledgments

I would like to express the deepest appreciation to my committee chair, Dr. Alexei Rybkin, who has motivated and guided me throughout the research process. Dr. Rybkin introduced me to the Shallow Water wave equations as well as the Carrier-Greenspan transformation and thus gave me most of the theoretical mathematical tools that were critical to my thesis. His criticism of my work has made me a better mathematician. If it were not for Dr. Rybkin's involvement this thesis would not have been possible.

I would also like to thank my committee member Dr. Dmitry Nicolsky for the many hours he spent discussing numerical schemes with me, showing me how to improve the schemes presented in this thesis, introducing me to some of the geophysical and numerical literature used in my thesis, teaching me to write professionally and critically reading my work. Dr. Nicolsky's involvement has been critical to my thesis and has greatly increased my abilities as an applied mathematician.

In addition I would like to thank Dr. Efim Pelinovsky for his introduction to the derivations of the shallow water wave equations and advice on how to set up the spectral solution – his advice has been invaluable, Dr. Ed Bueler for teaching me the mathematical analysis of finite difference methods through his course on the numerical solutions to PDEs, Dr. John Rhodes for teaching me the basics used in many of the optimization algorithms used throughout my work, Dr. Gordon Williams for his careful reading of my thesis and many suggestions on the best ways to organize my thought, and Slava Garayshin for his help on finding the eigenfunctions in Chapter 4. Financial support was given by the University of Alaska, Fairbanks and NSF Grant DMS 1009673.

Chapter 1

Introduction

Tsunami waves are long waves that pose a major hazard to coastal regions and can result in tremendous damages to affected communities. For example the 2004 Indian Ocean tsunami reportedly resulted in more than 228,000 deaths and an estimated 10 billion USD economic impact [BR09]. More recently the March 2011 Tohoku tsunami is reported to have caused 15,889 deaths and had an estimated economic impact of over 250 billion USD [Nat14, NCD11]. In order to mitigate damages tsunamis cause, potentially affected communities must be identified and emergency plans must be made. Since large underwater earthquakes could trigger a major tsunami, coastal communities near subduction zones have an increased risk for tsunami damages.

The Aleutian megathrust, where the Pacific plate is being subducted underneath the North American plate, has delivered numerous great earthquakes and is considered one of the most seismically active fault zones in the U.S. [RLK07, BDN⁺11]. Recently there have been many large earthquakes in the Aleutian megathrust. Notable large earthquakes are the M8.3 earthquake west of Kodiak Island in 1938, the M8.6 Andreanof Island event in 1957, the M9.2 Alaska earthquake in 1964, and the M8.7 Rat Island earthquake in 1965. These earthquakes ruptured almost the entire length of the megathrust and generated large tsunami waves that traveled for several hours and impacted exposed shorelines across the Pacific Ocean [GMO97, NGD13]. In particular the devastating 1964 tsunami struck the seaboard of southeast Alaska and then traveled into the narrow channels and canals further inland. The communities of Skagway and Haines located at the end of Lynn Canal were struck by

3.0 and 5.8 meter waves during the 1964 event [NGD13]. It is believed that the Aleutian megathrust has the greatest potential to generate tsunamis that would affect Alaska [DW08].

The impact of a tsunami depends on how well a community is prepared and on how efficient emergency managers can evacuate the near-shore areas. Depending on the information bulletin issued by Tsunami Warning Centers, emergency managers and harbor masters are recommended to take actions ranging from limiting access to the waterfront to a full evacuation of the near-shore areas [Ewi11, WAB⁺13]. Since over-evacuation may result in heavy costs to businesses, and potentially damage public confidence in response activities, emergency managers cannot simply use worst case scenarios to determine the evacuation plan [Kif12, WMew]. Because of this, a quick and robust assessment of the incoming tsunami is paramount to the determination of an emergency plan. To this effect, the Warning Centers process all available data to provide a forecast of the potential inundation at selected sites [TTC09]. Unfortunately at some locations (such as small coastal towns in Alaska) the only information available may be a near-shore tsunami height estimation [WAB⁺13]. Thus, quick and efficient estimates of the potential wave height at locations, where forecasts by the Warning Centers are not yet available, are important to select an appropriate evacuation procedure (R. Wilson, California Department of Conservation Agency and K. Miller, California Governors' Office of Emergency Services, personal communication, 2014). The process of finding the maximum/minimum values the wave height achieves at the shore is referred to as the tsunami runup/rundown problem. The runup is the maximum height and the rundown is the minimum wave height.

Recent studies of the 2011 Tohoku tsunami have suggested that the local bathymetry (U-shaped verses V-shaped) is a key component in predicting the local runup. V-shaped bays have larger runup than U-shaped bays [LST⁺13, SSO⁺12, KKP⁺13, SCP⁺14]. In light of these studies, an understanding of the runup characteristics in such bays may help communities where no warning center forecast is available.

The nonlinear shallow water theory in two dimensions is commonly used to predict the runup of long waves in coastal areas [SB06]. In the case of narrow, long channels and fjords,

the governing 2D equations can be simplified into a 1D system [Sto57, PT94, DP11b, RPD14]. Under this simplification the mass and linear momentum conservation principles become the so called shallow water wave equations (SWEs)

$$\frac{\partial S}{\partial t} + \frac{\partial}{\partial x}(uS) = 0, \quad (1.1)$$

$$\frac{\partial u}{\partial t} + u \frac{\partial u}{\partial x} + g \frac{\partial H}{\partial x} = g \frac{dh}{dx}. \quad (1.2)$$

Here, $u = u(x, t)$ is the cross-section averaged velocity, $\eta = \eta(x, t)$ and $h = h(x)$ are the water displacement and unperturbed water depth along the main axis of the bay, respectively. The quantity $H(x, t) = \eta(x, t) + h(x)$ is the total water depth, g is the acceleration of gravity, and $S(x, t)$ is the area of the water cross-section of the bay. We assume that S is a function of total depth H only; i.e. the cross-section of the bay does not change with respect to x . Figure 1.1 is a defining diagram in the particular case of a N -wave in a parabolic bay.

In 1957, Carrier and Greenspan developed a hodograph transform (known as the classical Carrier-Greenspan transform) from (1.1-1.2) into a linear second order wave equation in the case of a plane sloping beach (i.e. $h(x) = \alpha x$ for some constant $\alpha > 0$)[CG57]. The classical Carrier-Greenspan transformation has been an invaluable tool in the development of solutions to shallow water wave equations [Shu73, Spi76, Syn87, Syn91, PM92, TS94, Pel95, MP01, CWY02, Kan04, TT05, ZPGO06, Bar11]. In 2011, the Carrier-Greenspan transformation was generalized to sloping bays with parabolic cross-sections (i.e. bays with bathymetry of the form $Z(x, y) = y^2 + \alpha x$ for some constant $\alpha > 0$) and then to sloping bays with U-shaped cross-sections (i.e. bays with bathymetry of the form $Z(x, y) = |y|^m + \alpha x$ for some constants $m > 0$ and $\alpha > 0$)[DP11a, DP11b]. This generalization has led to an analytic solution for N -wave runup in a constantly sloping parabolic bay [DP11b], the development of a spectral solution for a parabolic bay of infinite length [DP11b], and a spectral solution for U-shaped bays of infinite length [Gar13]. Following the 2011 generalization, the Carrier-Greenspan transformation was generalized to the case of sloping bays with arbitrary cross-section [RPD14].

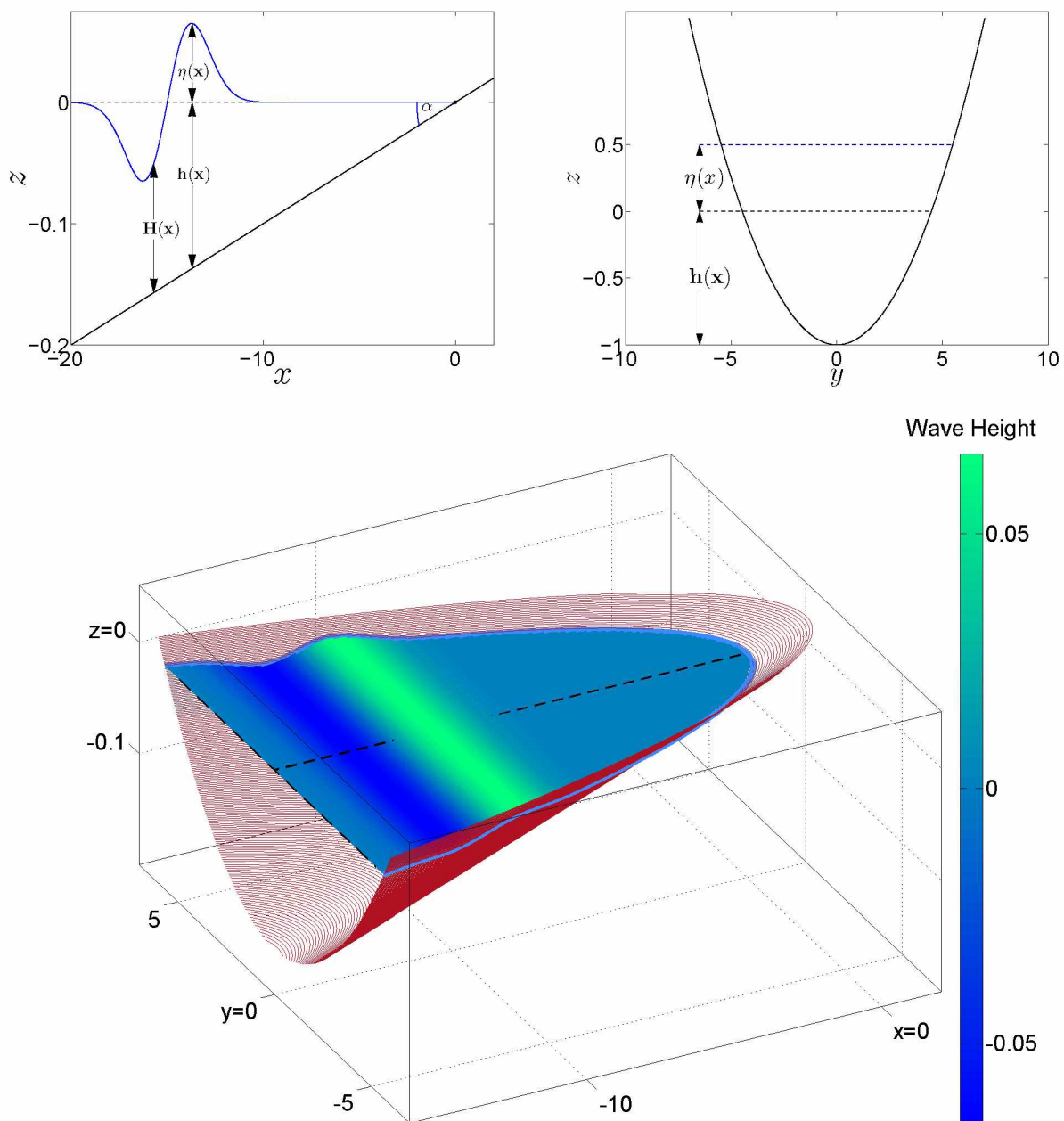


Figure 1.1: Top Left: a (x, z) cross-sectional view of an N -wave in a constantly sloping parabolic bay, Top Right: a (y, z) cross-sectional view of a parabolic bay with water displacement $\eta(x)$, and Bottom: the 3D view of the bay and N -wave given by the two cross-sections.

Because of the recent generalization of the Carrier-Greenspan transform as well as the recent interest in the runup characteristics of long waves in U and V shaped bays, a study of the viability of the generalized-Carrier transform as a numerical tool to study wave runup in such bays is of great interest. This paper will present two fast and accurate numerical methods that use the generalized Carrier-Greenspan transformation.

1.1 Chapter Overview

In Chapter 2 we give an overview of the generalized Carrier-Greenspan transform [RPD14]. Following our discussion of the generalized transformation we show how to compute the Carrier-Greenspan transformation for the case of U -shaped bays and present the analytic solution given in [DP11b]. We then develop a numerical method to implement the generalized transform as in [HNPR15].

In Chapter 3 we turn our attention to the development of a finite difference method to solve the linear system that results from the generalized Carrier-Greenspan transform. To test our method we compare the numerical solution given by our method to an analytic solution found by Didenkulova [DP11b]. This is followed by a comparison of our method to the 3D numerical solver FUNWAVE for the case of a N -wave runup in a trapezoidal bay. This work is the same as the work in [HNPR15].

In Chapter 4 we first develop an appropriate initial value boundary problem (IVBP) for wave runup in a U -shaped sloping bay with a wall located a finite distance from the shore. Our IVBP is similar to the work by [Bar11] and [KS06a]. We then use the Carrier-Greenspan transformation to find a spectral solution via the use of Sturm-Liouville theory. A numerical algorithm to utilize the spectral solution is then developed. This algorithm is tested by using an analytic solution.

The methods in Chapters 3 and 4 are significantly faster than similar numerical methods that are known to us.

Chapter 2

Carrier-Greenspan Transform

We give a brief overview of the generalized Carrier-Greenspan transformation. The key to be able to implement the Carrier-Greenspan transform is a function $F(\sigma)$. We thus discuss how to compute $F(\sigma)$ for two bays that are of interest. For the second bay $F(\sigma)$ cannot be found analytically suggesting that numerical methods are needed for many bays. We thus discuss how to numerically find $F(\sigma)$ and implement the Carrier-Greenspan transform.

2.1 Generalized Carrier-Greenspan Transformation

In this section, we provide a brief review of the generalized transformation by Rybkin et al. [RPD14] for a linearly inclined bay of arbitrary cross-sections. Following Rybkin et al. [RPD14] we assume that the bay bathymetry is determined by $Z = f(y) - h(x)$, where $f(y)$ describes the cross-section of the bay and $h(x)$ is restricted to $h(x) = \alpha x$ for some bay slope $\alpha > 0$. Since (1.1)-(1.2) forms a conservative system of two first order hyperbolic equations, it admits two characteristic curves and corresponding Riemann Invariants. Rybkin et al. found the Riemann invariants and corresponding characteristics to be $J_{\pm} = u \pm \int \sqrt{\frac{g}{S} \frac{dS}{dH}} dH$ and $c_{\pm} = u \pm \sqrt{gS \frac{dH}{dS}}$. With the characteristics and corresponding Riemann invariants known, Rybkin, et al. showed that equations (1.1) and (1.2) can be written in characteristic form as

$$\frac{\partial x}{\partial I_{\mp}} - c_{\pm} \frac{\partial t}{\partial I_{\mp}} = 0 \quad (2.1)$$

where $I_{\pm} = J_{\pm} + \alpha g t$ are modified Riemann Invariants. Consequently a new coordinate system (σ, λ) is defined in terms of the modified Riemann Invariants. In particular we define

$\lambda = (I_+ + I_-)/2$ and $\sigma = (I_+ - I_-)/2$, or

$$\lambda(x, t) = u(x, t) + \alpha g t, \quad \sigma(x, t) = \int_0^{H(x, t)} \sqrt{g} D(h) dh, \quad (2.2)$$

where

$$D(H) = \sqrt{\frac{\partial}{\partial H} (\ln S(H))}. \quad (2.3)$$

As seen by (2.2), the variable λ is related to time, while σ is associated with the spatial variable x . Note that at the shoreline $H(x, t) = 0$, and thus the shoreline location is associated with $\sigma = 0$. This is major advantage of the (σ, λ) coordinate system as the shoreline location in (x, t) coordinates varies for any nontrivial runoff problem. Now note that as $H(x, t)$ is non-negative, σ is as well. Finally note that if the initial water velocity $u_0(x, 0) = 0$ then $t = 0$ corresponds to $\lambda = 0$ for all x . Throughout this theses the (x, t) coordinate system will be referred to as physical coordinates and the (σ, λ) coordinate system will be referred to as nonphysical coordinates.

In order to exploit the convenient properties of the (σ, λ) coordinate system Rybkin, et al. [RPD14] introduced a function $F = F(\sigma)$ and the potential $\Phi = \Phi(\sigma, \lambda)$ such that

$$F(\sigma) = c_+ - c_- = \frac{2\sqrt{g}}{D(H(\sigma))}, \quad u = \frac{\Phi_\sigma}{F}. \quad (2.4)$$

In terms of (2.4) equation (2.1) becomes the linear system

$$\Phi_{\lambda\lambda} - \Phi_{\sigma\sigma} - W(\sigma)\Phi_\sigma = 0, \quad W(\sigma) = \frac{2 - F_\sigma}{F}. \quad (2.5)$$

Furthermore utilizing (2.2), (2.4) and the fact that $H(x, t) = \eta(x, t) + h(x)$ the transformation from the physical and nonphysical coordinate system can be found as

$$u = \frac{\Phi_\sigma}{F}, \quad \eta = \frac{1}{2g} (\Phi_\lambda - u^2), \quad x = \frac{1}{2g\alpha} (\Phi_\lambda - 2gH - u^2), \quad t = \frac{\lambda - u}{\alpha g}. \quad (2.6)$$

In order to solve (2.5), it is necessary to specify the initial conditions and boundary conditions. Typically, the initial water disturbance $\eta_0(x) = \eta(x, 0)$ and velocity $u_0(x) = u(x, 0)$ are available in terms of physical variables (x, t) and need to be transformed into the

initial conditions in (σ, λ) coordinates. Exploiting (2.6), we obtain

$$\Phi_\sigma(\sigma, 0) = u_0(x(\sigma, 0))F(\sigma), \quad \Phi_\lambda(\sigma, 0) = 2g\eta_0(x(\sigma, 0)) + u_0^2(x(\sigma, 0)), \quad (2.7)$$

where $x(\sigma, 0)$ can be found via (2.2). Finding the initial conditions for arbitrary $u_0(x)$ in sloping bays of arbitrary cross section is still an open research question. There has however been some research in the case of a plane sloping beach. In particular [KS06b] were able to find an analytic solution to the runup problem for arbitrary u_0 . For the solution techniques used in this paper the technique employed by [KS06b] can only be used when $\eta_0(x)$ is sufficiently small. For arbitrary $\eta_0(x)$ we thus limit the scope of this paper by assuming that $u_0 = 0$. Now to define the boundary condition at $\sigma = 0$, we note that $F(0) = 0$, and since the water velocity $u = \Phi_\sigma/F$ should be bounded we impose

$$\Phi_\sigma(0, \lambda) = 0. \quad (2.8)$$

The offshore boundary condition will be changed throughout the paper depending on if the bay is finite or infinite. In particular Chapter 3.1.1 will develop a boundary condition for a bay of infinite length and Chapter 4 will develop a boundary condition for a bay of finite length.

2.2 Computing $F(\sigma)$ for Bays of Interest

We will now demonstrate how one can compute $F(\sigma)$ for U and V shaped bays followed by a discussion of the complications in computing $F(\sigma)$ for bays of trapezoidal cross-sections. The complications for computing $F(\sigma)$ in the case of a bay with trapezoidal cross-sections is the motivation of the development of a numerical method that utilized the Carrier-Greenspan transformation.

2.2.1 $F(\sigma)$ for U and V Shaped Bays

For U and V shaped bays we are referring to a constantly sloping bay with cross sections of the form $f(y) = |y|^m$ for $m > 1$ and $0 < m \leq 1$ respectively. A sample U shaped bay for $m = 2$ (the so called parabolic bay) is shown in Figure 1.1. To compute $F(\sigma)$ for such bays, we must first find the cross-sectional area $S(H)$ for such bays. Since the only difference

between U and V shaped bays is the value of m , we will compute $F(\sigma)$ for both types of bays simultaneously. For a given height H the cross-sectional area $S(H)$ is given by

$$S(H) = 2 \int_0^{H^{1/m}} H - y^m dy = \frac{mH^{\frac{m+1}{m}}}{m+1}.$$

Thus $D(H)$ is computed via (2.3),

$$D(H) = \sqrt{\frac{S'(H)}{S(H)}} = \sqrt{\frac{m+1}{mH}}.$$

From (2.2) we compute $\sigma(H)$ and thus see that

$$H(\sigma) = \frac{m}{4g(m+1)}\sigma^2$$

and thus

$$D(H(\sigma)) = \frac{2\sqrt{g}(m+1)}{m\sigma}.$$

Finally we see that

$$F(\sigma) = \frac{m\sigma}{m+1}. \tag{2.9}$$

The key step in being able to analytically compute $F(\sigma)$ is finding $H(\sigma)$ analytically. We postulate that there are many bays where $F(\sigma)$ can not be found analytically.

2.2.2 $F(\sigma)$ for a Trapezoidal Bay

We now consider bays given by a trapezoidal channel. An example of such a channel is shown in Figure 2.1. We will define the quantity y_0 as half of the base length, and β as the slope of the lateral walls. Using the formula for the area of a trapezoid, we find that

$$S(H) = \frac{H^2}{\beta} + 2\beta y_0 H.$$

Thus, computing $D(H)$ using (2.3) we see that

$$D(H) = \sqrt{\frac{2H + 2\beta y_0}{H^2 + 2\beta y_0 H}}.$$

Now to find $H(\sigma)$ we must invert the function

$$\sigma = \int_0^H \sqrt{g} \sqrt{\frac{h + \beta y_0}{h^2 + 2\beta y_0 h}} dh.$$

Evaluation of this integral leads to an expression in terms of elliptic integrals of the second kind. It is well known that the elliptic integral of the second kind does not admit an analytic solution [AS65]. Because of this it was not possible to find $H(\sigma)$ analytically. Furthermore as trapezoidal bays are a simple extension of the V shaped bay given by cross-section $f(y) = |y|$, the lack of an analytically computable expression for $H(\sigma)$ suggest that there are many bays that lack an analytic expression for $F(\sigma)$. We now note that for all cross-sections $S'(H) > 0$ and thus $D(h) > 0$ for all $h > 0$, it then follows that $H(\sigma)$ is a well defined function for any cross-section.

2.3 Analytical Solution in a Parabolic Bay

One of the most valuable tools to verify numerical algorithms are analytical solutions. Such a solution allows one to explicitly compute the error of a numerical method. Throughout Chapters 3 and 4 we will need to have some solution to verify that our numerical algorithms are correctly computing wave runup. With this in mind we will discuss an analytical solution found by Didenkulova and Pelinovsky [DP11b] for the case of runup in parabolic bays. Given the initial condition in (σ, λ) coordinates

$$\eta_0(\sigma) = -\frac{4A}{gp^2} \left[\frac{\sigma - \sigma_0}{\sigma} e^{-\frac{(\sigma - \sigma_0)^2}{\rho^2}} + \frac{\sigma + \sigma_0}{\sigma} e^{-\frac{(\sigma + \sigma_0)^2}{\rho^2}} \right] \quad \text{and} \quad u_0(\sigma) = 0$$

where A represents the maximum wave height, σ_0 is the distance of the wave from the shore, and ρ is the wave length. Such a wave profile is called an N -wave because of its shape. Figure 2.2 shows a picture of $\eta(\sigma, 0)$ in terms of physical coordinates. For this initial profile Didenkulova and Pelinovsky found the following D'Alembert solution:

$$\Phi(\sigma \geq 0, \lambda) = \frac{A}{\sigma} \left[e^{-(\sigma + \lambda - \sigma_0)^2/p^2} - e^{-(\sigma - \lambda - \sigma_0)^2/p^2} + e^{-(\sigma + \lambda + \sigma_0)^2/p^2} - e^{-(\sigma - \lambda + \sigma_0)^2/p^2} \right].$$

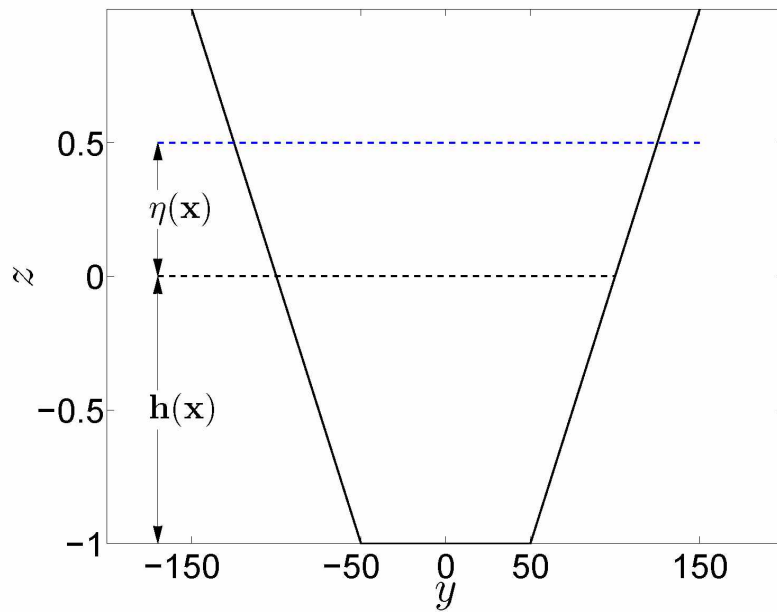
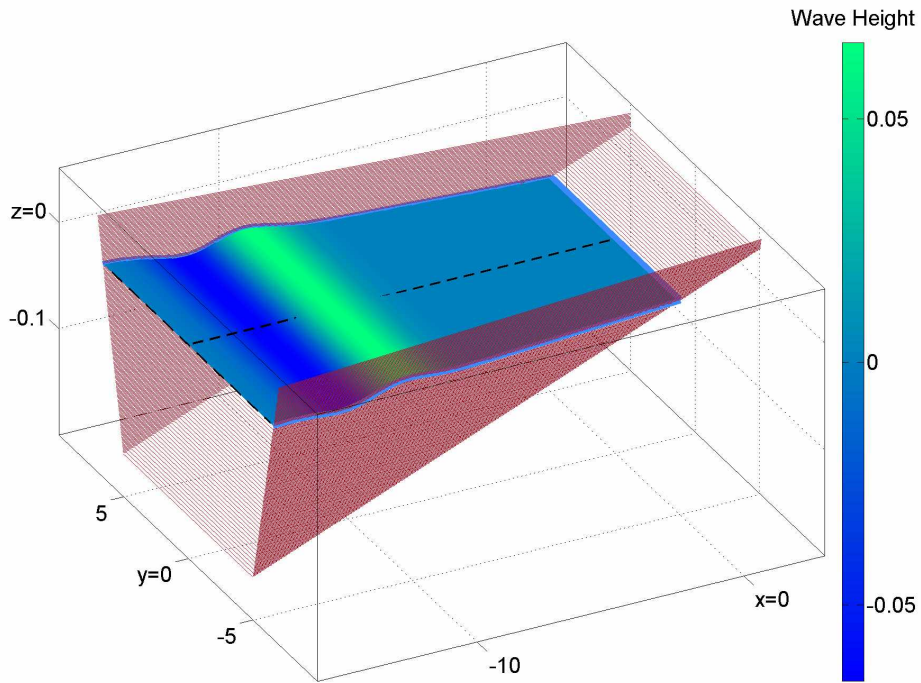


Figure 2.1: Top: A schematic view of a wave propagating in the trapezoidal beach with lateral walls slope $\beta = 1/2$, bottom width of $2y_0 = 100$ meters and the beach inclination of $\alpha = 0.01$. Bottom: a transverse cross-section of the bay.

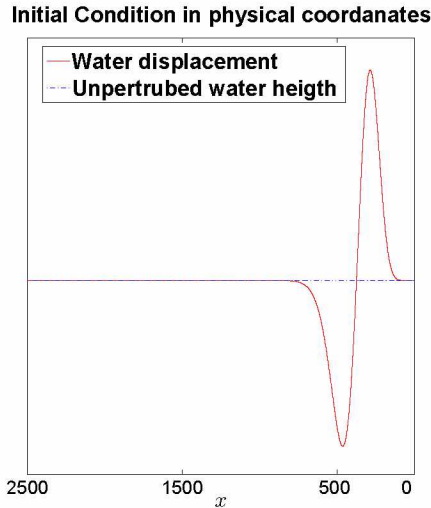


Figure 2.2: Initial condition in physical coordinates for an analytical solution for the runup problem in a parabolic bay.

Recalling that $F(\sigma) = (2/3)\sigma$ for a parabolic bay, to show that Φ is indeed a solution one must verify that

$$\eta(\sigma, 0) = \frac{1}{2g} \left(\Phi_{\lambda}(\sigma, 0) - 4/9 \left(\frac{\Phi_{\sigma}(\sigma, 0)}{\sigma} \right)^2 \right)$$

and that

$$\Phi_{\lambda\lambda} - \Phi_{\sigma\sigma} - \frac{2}{\sigma} \Phi_{\sigma} = 0.$$

These are straight forward calculations that are quite tedious so we will omit the details here. The interested reader is referred to [DP11a] for a derivation of this analytic solution.

2.4 Numerical Implementation of the Carrier-Greenspan Transformation

In order to utilize the Carrier-Greenspan transformation we must numerically realize the transformation between physical and nonphysical coordinates. We first show how to convert from initial physical coordinates into nonphysical coordinates and then how to convert back to physical coordinates.

The main challenge in converting to nonphysical coordinates is computing $F(\sigma)$ and $F_\sigma(\sigma)$ for an arbitrary sloping bay. For numerical purposes we need to develop a method to find $F(\sigma)$ and $F_\sigma(\sigma)$ for any set of points $\{\sigma_k\}_{k=1}^N$. To do this, we note that the function F can be explicitly obtained in terms of H via (2.4). Thus to compute $F(\sigma_k)$, the function $H(\sigma_k)$ needs to be known. As was discussed in Section 2.2.2, $H(\sigma)$ may not be computable as an analytic function since the equation $\sigma(x, t) = \int_0^{H(x,t)} \sqrt{g}D(h)dh$ may not be analytically invertible. To resolve this problem we turn to numerical methods. In particular for a given σ_k we numerically solve

$$\sigma_k(x, t) - \int_0^{H_k} \sqrt{g}D(h)dh = 0$$

for H_k via the Newton-Raphson method. With $F(\sigma_k)$ known, $F_\sigma(\sigma_k)$ is then computed via the finite difference method (i.e. $F_\sigma(\sigma_k) \approx (F(\sigma_k + \Delta\sigma) - F(\sigma_k - \Delta\sigma))/(2\Delta\sigma)$).

Once $F(\sigma)$ and $F_\sigma(\sigma)$ are known, $\Phi_\sigma(\sigma(x, t), \lambda(x, t))$ and $\Phi_\lambda(\sigma(x, t), \lambda(x, t))$ can be computed from (2.7) and $\lambda(\sigma(x, t), \lambda(x, t))$ can be computed via (2.6). Furthermore $\sigma(x, t)$ can be found through (2.2).

Once in nonphysical space the wave runup can be computed by solving (2.5). Methods to solve (2.5) are the subject of Chapters 3 and 4. With the wave runup known, we compute $\Phi_\sigma(\sigma, \lambda)$ and $\Phi_\lambda(\sigma, \lambda)$ via second order finite differences. With $\Phi_\sigma(\sigma, \lambda)$ and $\Phi_\lambda(\sigma, \lambda)$ along with $F(\sigma)$ known, equation (2.6) is used to first compute u , then η and finally x and t .

2.5 Conclusions

The most recent generation of the Carrier-Greenspan transformation greatly extends the range of problems that can be addressed. The method in 2.4 allows one to utilize the Carrier-Greenspan transformation for numerical experiments. In particular, runup in U and V shaped bays can now be addressed by solving a linear wave equation with analytically known nonconstant coefficients and converting back to physical coordinates. Furthermore for any constantly sloping bay with constant cross-sections, the generalized Carrier-Greenspan transformation allows one to numerically solve a linear wave equation to compute the wave runup.

Chapter 3

Numerically Solving the SWEs in an Infinite Sloping Bay with Constant Cross-Sections

As discussed in section 2.4, a method is needed to compute the wave runup in nonphysical coordinates. This chapter develops a robust finite difference method (referred to as the semianalytic method) that is valid for any sloping bay with some fixed arbitrary cross-section. We then demonstrate the validity of our method by comparing our method to the analytical solution discussed in Chapter 2.3. This is followed by two comparisons of our method to the verified and validated 3D numerical solver FUNWAVE.

For the comparison to the analytic solution, we use the maximum relative error throughout our domain as the metric for the models agreeing. This metric is appropriate as we are directly comparing our method to that of an analytic solution. Furthermore for the numerical comparison we will use the maximum runup as our comparison metric. This metric is appropriate as FUNWAVE is solving a different system (3D vs. 2D averaged) and thus it would not be expected that the two solutions would agree everywhere.

It is extremely notable that FUNWAVE takes approximately 2 CPU days to run (on a single core a8-5600k processor) and our method takes 2 CPU minutes (on a single core a8-5800k).

3.1 Numerical Algorithm for Runup in Bays of Infinite Length

Here we present a finite difference method for computing wave runup in the non-physical system (equation (2.5)). In the case of U and V shaped bays $W(\sigma) = (m + 2)/(m\sigma)$. From this expression we immediately see that $\sigma \rightarrow 0^+$ implies $W(\sigma) \rightarrow \infty$ and furthermore when $\sigma \rightarrow \infty$, $W(\sigma) \rightarrow 0$. The primary obstacle that must be overcome when solving (2.5) is

the singularity in $W(\sigma)$ at $\sigma = 0$. Thus we split (2.5) into a system of coupled PDES. The resulting coupled system is more numerically stable and allowed for the development of a stable finite difference method.

3.1.1 Development of an Initial Value Boundary Problem (IVBP)

To avoid the singularity at $\sigma = 0$, the auxiliary functions $\varphi = \Phi_\lambda$ and $\psi = \Phi_\sigma$ are introduced. With these new functions direct substitution shows that (2.5) becomes

$$\varphi_\lambda - \psi_\sigma - W(\sigma)\psi = 0. \quad (3.1)$$

Differentiating equation (3.1) in respect to σ and using Young's theorem (i.e. $\varphi_\sigma = \psi_\lambda$), one obtains

$$\begin{aligned} \Phi_{\sigma\lambda\lambda} &= \Phi_{\sigma\sigma\sigma} + W(\sigma)\Phi_{\sigma\sigma} + W'(\sigma)\Phi_\sigma \\ \psi_{\lambda\lambda} &= \psi_{\sigma\sigma} + W(\sigma)\psi_\sigma + W'(\sigma)\psi. \end{aligned} \quad (3.2)$$

Equations (3.1)-(3.2) form a coupled system that is equivalent to our original system. Thus by numerically solving (3.1)-(3.2) we can find the solution to (2.5).

For this system, the method developed in Chapter 2.4 enables us to find the non-physical analog of the initial wave height (Φ_λ) and initial wave velocity (Φ_σ) for small initial velocities. These conditions are

$$\varphi(\sigma, 0) = \Phi_\lambda(\sigma, 0) \text{ and } \psi(\sigma, 0) = \Phi_\sigma(\sigma, 0) \quad (3.3)$$

respectively. Furthermore the boundary condition at the moving shoreline given in (2.8) becomes

$$\Phi_\sigma(0, \lambda) = \psi(0, \lambda) = 0. \quad (3.4)$$

We now need to find a boundary condition for the offshore boundary.

To match the work done by Pelinovsky et al. [DP11b, RPD14], we wish to have a boundary condition that simulates a wave in an sloping bay of infinite length. If we fix some point $\sigma = \sigma_1$ such that $\sigma_1 \gg 1$ then $W \approx 0$. Consequently equation (3.2) can be approximated by the linear wave equation $\psi_{\lambda\lambda} = \psi_{\sigma\sigma}$. Therefore, a wave traveling away

from the shore at $\sigma = \sigma_1$ can be approximated via the one directional wave equation

$$\psi_\lambda(\sigma_1, \lambda) = -\psi_\sigma(\sigma_1, \lambda). \quad (3.5)$$

We note that the choice to expand $\frac{d}{d\sigma}(W(\sigma)\psi)$ in (3.2) was to facilitate the enforcement of the boundary condition $\psi(0, \lambda) = 0$ at the origin.

We now develop a numerical method to solve (3.1)-(3.2) with the initial conditions (3.3) and boundary conditions (3.4)-(3.5).

3.1.2 Numerical Algorithm

With any numerical method to solve a partial differential equation, the stability condition is a major restriction. For our system the Courant-Friedrichs-Lewy (CFL) stability condition for explicit finite difference methods [CFL28] imposes severe requirements on the time step near the origin. In particular the CFL condition requires our time step to approach 0 whenever a wave approaches the shoreline. These restrictions mean that it is not feasible to apply an explicit finite difference scheme to (3.2). We thus choose to apply an implicit method to (3.2) [Fle91]. To compute $\psi_{\lambda\lambda}$, we employ the second order central difference formula

$$\psi_{\lambda\lambda}(\lambda, \sigma) = \frac{\psi(\lambda + \Delta\lambda, \sigma) - 2\psi(\lambda, \sigma) + \psi(\lambda - \Delta\lambda, \sigma)}{\Delta\lambda^2}.$$

The boundary condition (3.5) is discretized by first order one sided differences in both time and space (i.e. $(\psi(\lambda + \Delta\lambda, \sigma) - \psi(\lambda, \sigma))/\Delta\lambda = -(\psi(\lambda, \sigma + \Delta\sigma) - \psi(\lambda, \sigma))/\Delta\sigma$) and the boundary (3.4) is computed directly. We reiterate that one major factor expanding (3.2) is to allow the boundary condition (3.4) to be computed directly.

A numerical scheme for a second order PDE requires knowledge of the initial condition at two consecutive time steps. The initial condition $\psi(\sigma, 0)$ is readily available via the method outlined in Chapter 2.4. To obtain an approximation to ψ at the second time step, i.e. at $\lambda = \Delta\lambda$ we apply a Taylor series expansion

$$\psi(\sigma, \Delta\lambda) = \psi(\sigma, 0) + \Delta\lambda\psi_\lambda(\sigma, 0) + \psi_{\lambda\lambda}(\sigma, 0)\Delta\lambda^2/2 + O(\Delta\lambda^3).$$

We now note that

$$\psi_\lambda(\sigma, 0) = \Phi_{\sigma\lambda}(\sigma, 0) = \frac{d}{d\sigma}(2g\eta(\sigma, 0) + u^2(\sigma, 0))$$

and that

$$\psi_{\lambda\lambda}(\sigma, 0) = \Phi_{\sigma\lambda\lambda}(\sigma, 0) = \frac{d^2}{d\sigma d\lambda}(2g\eta(\sigma, 0) + u^2(\sigma, 0)) = 0.$$

Thus our second initial condition becomes

$$\psi(\sigma, \Delta\lambda) = \psi(\sigma, 0) + \Delta\lambda(2g\eta_\sigma(\sigma, 0) + 2u(\sigma, 0)u_\sigma(\sigma, 0)) + O(\Delta\lambda^3). \quad (3.6)$$

Note that $\psi(\sigma, \Delta\lambda)$ can be approximated with third order accuracy and our numerical scheme is at least second order accurate in space and time.

Now for any discretization of the domain in the form $\{k\Delta\sigma, l\Delta\lambda\}_{k=0, l=0}^{n, m}$ where $\Delta\sigma$ and $\Delta\lambda$ are the spatial and temporal discretization intervals for non-physical variables, we can compute $\psi(k\Delta\sigma, l\Delta\lambda)$ by applying the above method. Once the solution $\psi(k\Delta\sigma, l\Delta\lambda)$ is found, we compute φ at the same points by numerically solving (3.1). In particular φ_λ is discretized by a forward first order finite differences (i.e. $\varphi_\lambda(\sigma, \lambda) \approx (\varphi(\sigma, \lambda + \Delta\lambda) - \varphi(\sigma, \lambda))/\Delta\lambda$), while ψ_σ is computed by a central second order difference (i.e. $\psi_\sigma(\sigma, \lambda) \approx (\psi(\sigma + \Delta\sigma, \lambda) - 2\psi(\sigma, \lambda) + \psi(\sigma - \Delta\sigma, \lambda))/\Delta\sigma^2$) to preserve the overall accuracy of the numerical calculations. Finally, once the values of $\varphi(k\Delta\sigma, l\Delta\lambda)$ and $\psi(k\Delta\sigma, l\Delta\lambda)$ are computed, we apply our method for the inverse transformation outlined in Chapter 2.4. In general the points $\{x, t\}_{kl} = \frac{1}{2g\alpha}\varphi(k\Delta\sigma, l\Delta\lambda)$ will not have a uniform stepping in both the x and t directions. This is because the mapping from (σ, λ) to (x, t) is nonlinear. Thus, in order to compute profiles of the water height η at constant time, we employ the Delaunay triangulation algorithm in Matlab [MAT11] and linearly interpolate (η, u) between the nodes $\{x, t\}_{kl}$.

The choice of using Delaunay triangulation to transform the solution from $(k\Delta\sigma, l\Delta\lambda)$ to $\{x, t\}_{kl}$ is much faster than the Newton-Raphson method employed by [Kan04] and [KS06b] with only a small cost to accuracy. It is notable that we only use the Newton-Raphson method to calculate F_k and W_k and not the time series at specific location or spatial variation at specific time as Synolakis and others have done [Syn87]. The difference in using a

Delaunay triangulation as opposed to Newton-Raphson method to calculate the runup on an even grid leads to a great improvement of the speed of our method over previous methods.

Putting all of our work together, our algorithm for calculating wave dynamics is as follows

1. Given σ_k , compute H_k in order to find F_k , $(F_\sigma)_k$ and finally W_k and $(W_\sigma)_k$.
2. Setup the initial condition $\psi(\sigma_k, 0)$ according to (3.3).
3. Compute $\psi(\sigma_k, \lambda_1)$ at the second time step $\lambda_1 = \Delta\lambda$ according to (3.6).
4. Find $\psi(\sigma_k, \lambda_l)$ for consecutive time steps $l \geq 2$ according to the presented finite difference method for (3.2).
5. Compute $\varphi(\sigma_k, \lambda_l)$ for $k, l \geq 1$ according to the presented finite difference method for (3.1).
6. Use $\varphi(\sigma_k, \lambda_l)$, $\psi(\sigma_k, \lambda_l)$, F_k , and H_k to find $u(x_k, t_l)$, and $\eta(x_k, t_l)$ via (2.6).
7. Find the values of runup R_u and rundown R_d using $\eta(x_k, t_l)$ and optionally interpolate $\eta(x_k, t_l)$, $u(x_k, t_l)$ to uniformly spaced points (x, t) to produce indentation maps (space time diagrams for the wave runup).

3.2 Verification and Validation of the Numerical Method

We now check the accuracy of the algorithm presented in Chapter 3.1.2. In particular we run two numerical experiments: one in a parabolic bay with the initial condition given in Figure 2.2 and one in a trapezoidal bay with the same initial condition as Figure 2.2. The first experiment is compared to the analytical solution discussed in Chapter 2.3 and the second experiment is compared to the 3D numerical solver FUNWAVE.

3.2.1 Verification in a Parabolic Bay

Recall that Didenkulova and Pelinovsky [DP11b] found an analytic solution for the case of the wave given by the initial profile $\eta(\sigma, 0) = \frac{2A(\sigma - \sigma_0)}{2gp^2} e^{-(\sigma - \sigma_0)^2/p^2}$ in a constantly sloping parabolic bay (Chapter 2.3). To test our method, we will use the initial profile defined by

the constants $A = 0.5$, $p = 1.5$ and $\sigma_0 = 15$. The choice of these particular constants is to follow the work done by Didenkulova and Pelinovsky. The bottom picture in Figure 1.1 shows the scaled initial wave profiles in a parabolic bay with bay slope $\alpha = .1$. The propagation of the solitary wave towards the shore and its reflection is depicted in Figure 3.1. The shoreline is clearly fixed at the point $\sigma = 0$ in the nonphysical system. On the other hand the shoreline moves with the wave height in physical coordinates (x, t) with the largest deviations of the shoreline from its initial position occurring at runup and rundown. Furthermore in the nonphysical coordinate system, the wave characteristics can be clearly seen as straight lines as opposed to the parabolic like characteristic curves in the physical system. This linearization of wave characteristics is the key to the Carrier-Greenspan transformation.

For this parabolic sloping bay it has analytically derived that the values of runup and rundown are $R_u = 8Ae^{-3/2}/3p^2$, $R_d = -4A/3p^2$, respectively [DP11b]. For the above-mentioned values of A, p, σ_0 , the maximum wave runup is $R_u \approx 0.1322$ and the minimum wave rundown is $R_d \approx -0.2963$. We will denote the computed runup/rundown by \tilde{R}_u and \tilde{R}_d respectively. Tables 3.1 and 3.2 list the relative error in the computed runup and rundown for several different combinations of $\Delta\lambda$ and $\Delta\sigma$. Figure 3.2 graphically shows the points in Tables 3.2 and 3.1. In both tables it is notable that the error decreases rapidly as we decrease both $\Delta\sigma$ and $\Delta\lambda$ together. The effect of decreasing $\Delta\lambda$ on the error is greater than the effect of $\Delta\sigma$. This is primarily because our model is overall first order in computing φ in respect to $\Delta\lambda$ but quadratic in terms of $\Delta\sigma$; Thus when decreasing $\Delta\sigma$ (with $\Delta\lambda = \text{constant}$) our method converges to the solution much quicker than when $\Delta\lambda$ (with $\Delta\sigma = \text{constant}$) is decreased. Furthermore since the maximum runup and minimum rundown times are not known but their spatial location is always at the moving shoreline ($\sigma = 0$), decreasing $\Delta\lambda$ increases the number of time samples where we compute the runup/rundown whereas decreasing $\Delta\sigma$ does not. This increased sampling rate can easily affect the apparent convergence our method.

Tables 3.1 and 3.2 show that our method agrees with the analytical solution as we refine our grid. These tables can be easily visualized in Figure 3.2.

To further test our method we run several models leaving every parameter fixed other than the wave height. We then compute the maximum relative error of each model and examine how the relative error changes as a function of the wave height. It is notable that

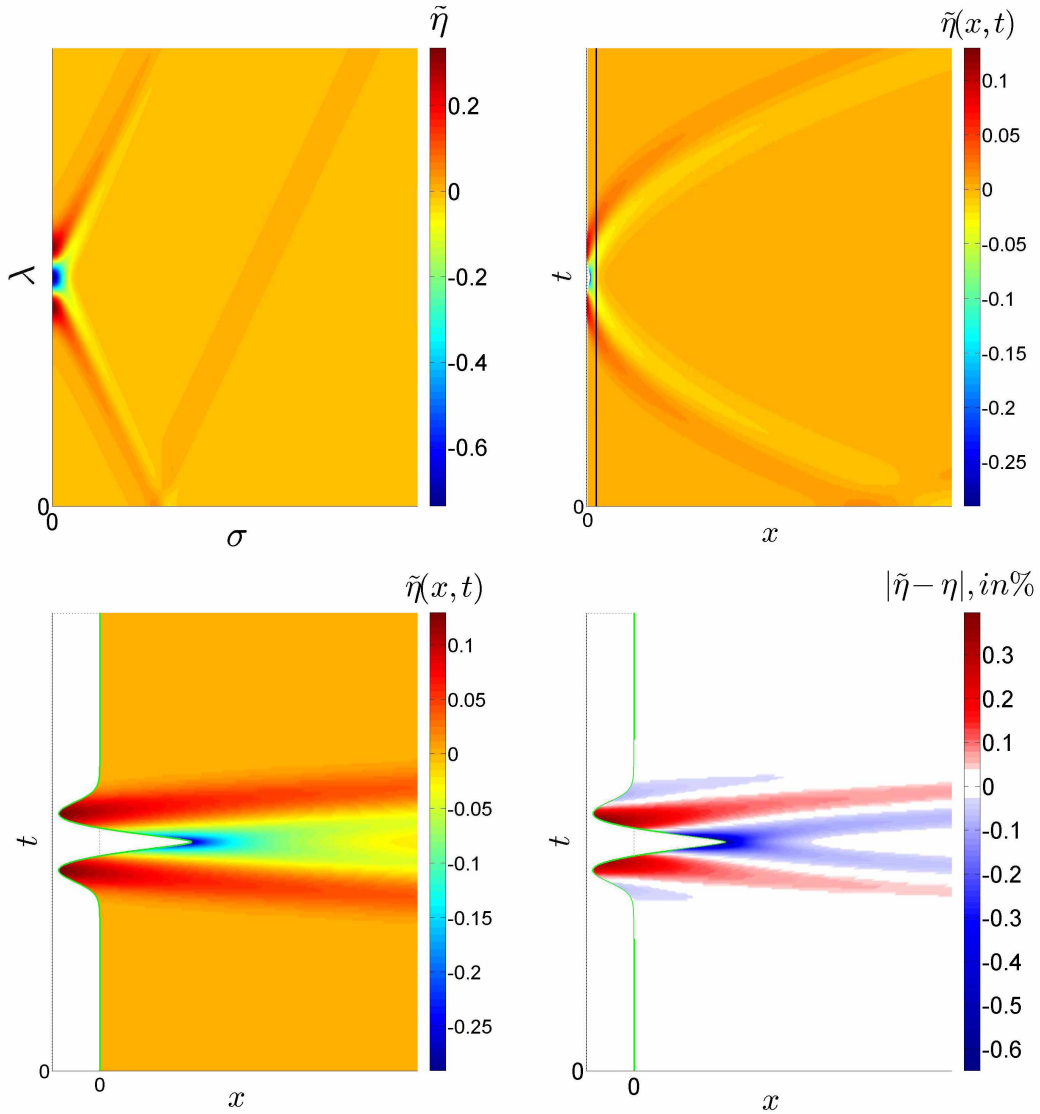


Figure 3.1: Top Left: the numerically computed wave dynamics in non-physical coordinates (σ, λ) . The shoreline is fixed at $\sigma = 0$. Top Right: the numerically computed wave dynamics in physical coordinates (x, t) . Bottom Left: the shoreline dynamics of the physical wave by restricting the x axis to $[-1.5, 20]$. The shoreline varies around $x = 0$. Bottom Right: the discrepancy between the analytical and numerical solution in the physical coordinates. The maximum errors occur at the runup (0.35%) and rundown (0.65%).

Table 3.1: The relative error $\|R_u - \tilde{R}_u\|/R_u$ in the runup for different values of $\Delta\lambda$ and $\Delta\sigma$ values.

Model Runup error with $(\Delta\lambda, \Delta\sigma)$	$\Delta\sigma = 1$	$\Delta\sigma = 0.1$	$\Delta\sigma = 0.01$	$\Delta\sigma = 0.005$
$\Delta\lambda = 1$	0.897372	0.896429	0.896429	0.896429
$\Delta\lambda = 0.1$	0.722520	0.690126	0.686332	0.686299
$\Delta\lambda = 0.01$	0.295066	0.178941	0.156491	0.156278
$\Delta\lambda = 0.001$	0.213095	0.085676	0.021997	0.021711
$\Delta\lambda = 0.0001$	0.204251	0.006944	0.004869	0.004573

Table 3.2: The relative error $\|R_d - \tilde{R}_d\|/R_d$ in the rundown for different values of $\Delta\lambda$ and $\Delta\sigma$ values.

Model Rundown error with $(\Delta\lambda, \Delta\sigma)$	$\Delta\sigma = 1$	$\Delta\sigma = 0.1$	$\Delta\sigma = 0.01$	$\Delta\sigma = 0.005$
$\Delta\lambda = 1$	0.959926	0.959926	0.959901	0.959900
$\Delta\lambda = 0.1$	0.823982	0.718481	0.716881	0.716866
$\Delta\lambda = 0.01$	0.685179	0.180632	0.171168	0.171078
$\Delta\lambda = 0.001$	0.663355	0.032658	0.019835	0.019714
$\Delta\lambda = 0.0001$	0.661000	0.015407	0.002167	0.002042

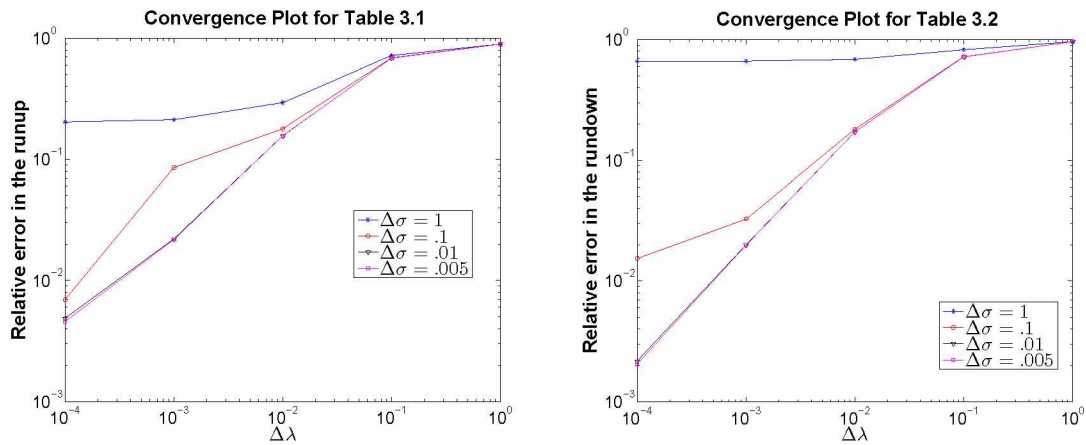


Figure 3.2: Left: loglog plot showing the errors given in Table 3.1, Right: loglog plot showing the errors given in Table 3.2

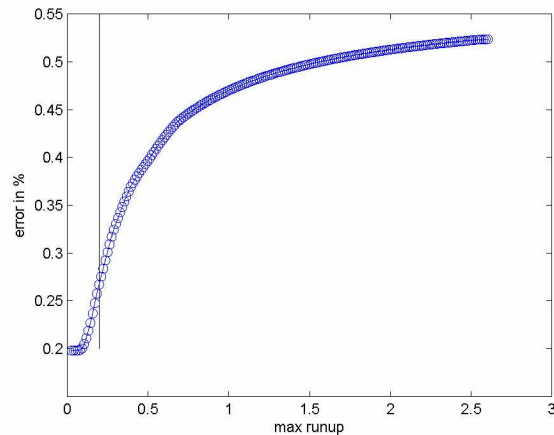


Figure 3.3: Relative error in the semianalytic method in a parabolic bay as a function of wave height. Note that the only factor that is changing in our semianalytic model is the initial wave height and that the error is always below .5% relative error. Furthermore the rate of change in the relative error decreases as the wave height increases.

as the wave height increase, the ratio of the wave height and the wave length grows. Thus for large amplitudes, the waves become less shallow. Figure 3.3 shows the relative error for different wave amplitudes.

3.2.2 Validation in a Trapezoidal Bay

In the last section we verified our algorithm using an analytic solution in the case of a parabolic bay. Since real world problems do not typically have analytical solutions as demonstrated by the lack of an analytical expression for a trapezoidal bay in Chapter 2.2.2, we will validate our numerical model in the case of wave runup in a trapezoidal bay. To validate our model we choose to compare the results of our model to the 3D numerical model FUNWAVE. We choose to use FUNWAVE to verify our method because FUNWAVE was verified and validated by [TKMS12, TSK⁺12] according to an exhaustive suite of tests proposed by [SBT⁺08]. We note that FUNWAVE employs the Total Variation Diminishing finite volume scheme [Tor09] along with adaptive Runge-Kutta time stepping [GST01] to model the propagation of the water waves. The interested reader can consult [SKH⁺12] for further details about the FUNWAVE model. It is important to mention that FUNWAVE gives the user the

option to take into account the wave dispersion [SKH⁺12]. Since the SWEs (1.1)-(1.2) are a non-dispersive system, we restrict FUNWAVE to non-dispersive behavior in our validation.

In order to validate our method on a realistic scenario, we assume an initial wave profile that is typically caused by a small submarine landslide at the head of a trapezoidal fjord. Typically, if some ground material fails at the head of the bay, the material then slides down along the fjord wall and consequently generates an N -wave with a leading depression. A conceptual picture of this phenomenon is shown in Figure 3.4. The initial and final positions of the slide are marked by letters A and B respectively and the resulting N -wave is shown in blue.

We thus assume an initial N-shaped wave with an amplitude of 10 cm has formed 1000 meters away from the shore in a trapezoidal bay with wall slope $\beta = 1/2$, bottom slope $\alpha = 0.05$ and width of 100 meters, i.e. $y_0 = 50$. It is notable that this bay is very similar to the steep glacial fjords typical of those found in Alaska, south-central Chili [FPC⁺11], and also very similar to the Pago Pago bay in American Samoa [FBS⁺11, Did13]. The geometry of the idealized channel and wave profile are shown in Figure 2.1.

In FUNWAVE, we simulate the propagation and runup of the same N-shaped wave with the trapezoidal bay in Figure 2.1. When the dispersive effects are turned off, FUNWAVE solves the classical 2-D shallow water equations, while the proposed semi-analytical model computes the cross-section averaged characteristics of the flow. In order to compare the results of the two models, we choose to compare our models results to FUNWAVE's results taken from the middle of the bay (see dashed line in Figure 2.1).

For the wave and bay in question we compute the maximum runup $R_u = 0.9500$ cm and minimum rundown $R_d = -.04753$ cm in FUNWAVE. We then compute the maximum runup \tilde{R}_u and minimum rundown \tilde{R}_d in our semi-analytic model. Tables 3.3 and 3.4 demonstrate the convergence of \tilde{R}_u and \tilde{R}_d respectively. Similar to the previous model these table show an apparent linear convergence in respect to $\Delta\lambda$ and quadratic convergence in respect to $\Delta\sigma$. Considering the significant differences between the two models (2D averaged water flow vs. 3D numerical flow), the predictions of the runup/rundown for the two models are close

A cross-sectional view of a bay with a submarine landslide.

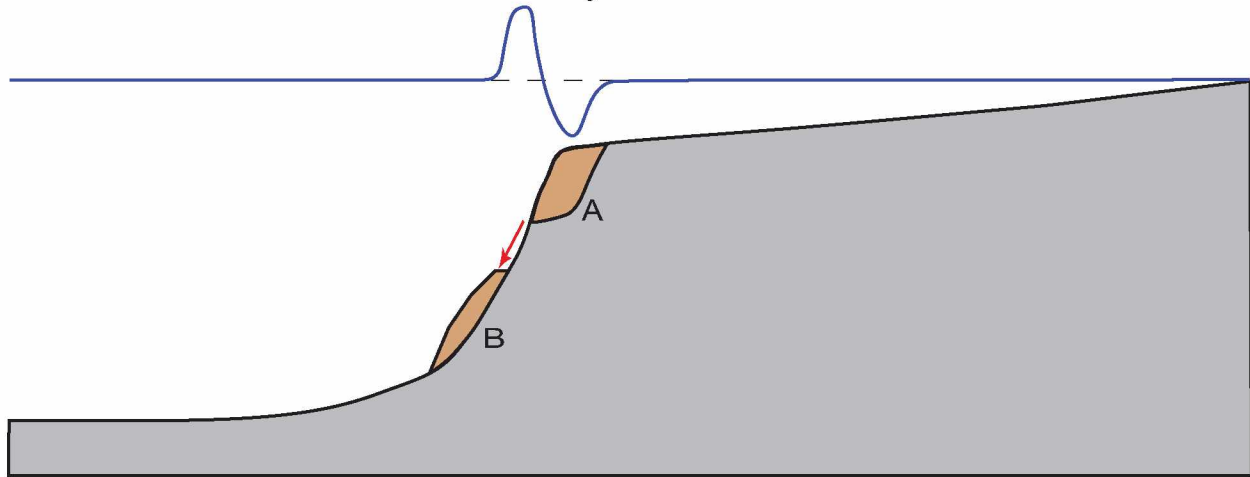


Figure 3.4: Schematic description of a submarine landslide. The landslide quickly moves material from its original location (A) to its resting location (B). This movement typically generates a N-wave.

to each other having 2.8% relative error in their runup values and 15.2% relative error in their rundown values.

It is notable that our numerical method is much faster than FUNWAVE (2 minutes vs. 2 hours).

We now compare the wave dynamics between the two models. Figure 3.5 compares the water level, η , computed by the semi-analytical model and FUNWAVE (at the center of the bay). Notice the discrepancy between the two models for certain time periods. In the top plot as the waves approach the beach there is only a small discrepancy near the center of the *N*-wave. The second plot from the top shows the minimum rundown that the waves achieve. There is still only a small difference in the models at this point in the simulations. This between the models grows greatly ten seconds after the minimum rundown is achieved as seen in the third plot. It is notable that it is only near the shoreline where the two models differ in the third plot. Only 8 seconds later when the waves have reached their maximum runup, the models once again are in good agreement. The fourth plot shows this comparison. Furthermore as the wave continues to propagate the discrepancy returns as shown in the fifth plot. Finally, in the bottom plot, after the wave reflects from the shore, the discrepancy is

Table 3.3: Convergence of the \tilde{R}_u computed by the semi-analytical model. Note that the rundown in the FUNWAVE simulation is 0.9500 cm.

Model Runup with $(\Delta\lambda, \Delta\sigma)$	$\Delta\sigma = 1$	$\Delta\sigma = .1$	$\Delta\sigma = .01$	$\Delta\sigma = .005$
$\Delta\lambda = 1$	0.1890	0.1910	0.1910	0.1910
$\Delta\lambda = .1$	0.6900	0.7205	0.7209	0.7209
$\Delta\lambda = .01$	0.8473	0.8994	0.9001	0.9001
$\Delta\lambda = .001$	0.8662	0.9207	0.9214	0.9215
$\Delta\lambda = .0001$	0.8682	0.9229	0.9236	0.9236

Table 3.4: Convergence of \tilde{R}_d computed by the semi-analytical model. Note that the rundown in the FUNWAVE simulation is -0.4069 cm.

Model Rundown with $(\Delta\lambda, \Delta\sigma)$	$\Delta\sigma = 1$	$\Delta\sigma = .1$	$\Delta\sigma = .01$	$\Delta\sigma = .005$
$\Delta\lambda = 1$	-0.0998	-0.1000	-0.1000	-0.1000
$\Delta\lambda = .1$	-0.3694	-0.3643	-0.3643	-0.3643
$\Delta\lambda = .01$	-0.4774	-0.4614	-0.4613	-0.4613
$\Delta\lambda = .001$	-0.4916	-0.4741	-0.4740	-0.4740
$\Delta\lambda = .0001$	-0.4931	-0.4754	-0.4753	-0.4753

still present but not as large as it was at the shoreline. Despite these discrepancies, the models agree on the time of maximum runup/ minimum rundown and give close to the same magnitude of the max runup (0.9236 cm vs. 0.9500 cm in FUNWAVE)/ min rundown(-.4753 cm vs. -.4069 cm in FUNWAVE). It is notable that even though our semianalytic model is an averaged 2D model, many of the features of the fully 2D model are present in our semianalytic model.

3.3 Conclusions

The numerical method developed can quickly and accurately compute tsunami runup. It has been verified and validated against the analytical solution given in Chapter 2.3 and a well tested 3D numerical model. The results of these tests showed that our method accurately computes wave runup with a slight time difference for the outgoing wave. We believe that time warping is the result of the differences between the fully 3D SWEs and the cross-sectional averaged SWEs but more research is required to confirm this.

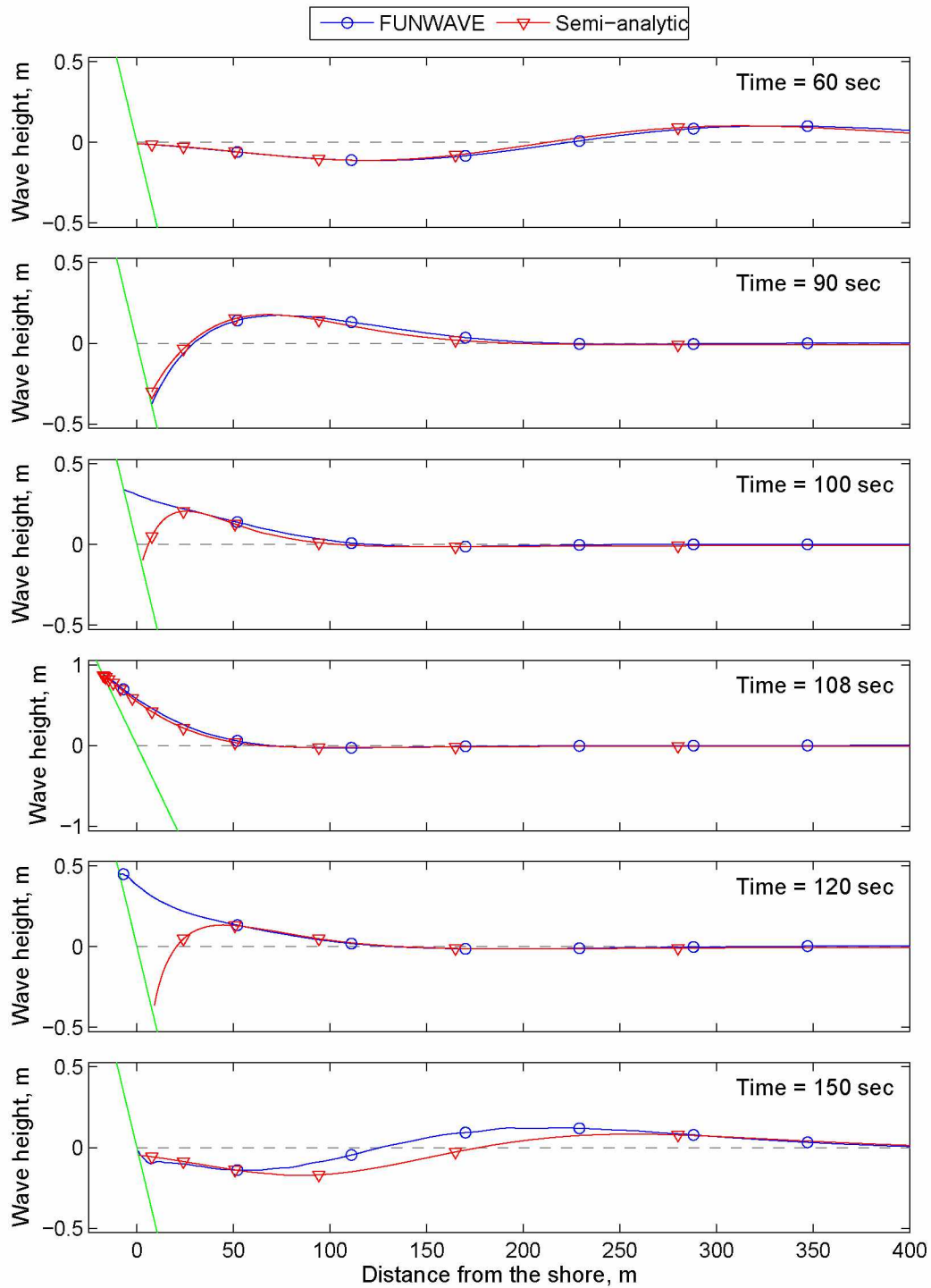


Figure 3.5: Comparison of the water level computed by the semi-analytic and FUNWAVE models.

This shows that the generalized Carrier-Greenspan is a valid method for computing wave runup and that our algorithm for computing the transformation between coordinates is valid. Furthermore the speed of our model as compared to the 3D model FUNWAVE (semianalytic is about 2,800x faster) suggest that our method is a viable option if a quick approximation for tsunami runup is needed. This method thus has the potential to quickly compute approximations to real world tsunami runup problems and may be a valuable tool to extend the range of cities that have a tsunami runup forecast.

Chapter 4

Spectral Solution for U and V Shaped Bays of Finite Length

In this chapter, we develop another method to solve the resulting linear system (2.5) with the initial conditions (2.7) and the boundary condition (2.8). As in Chapter 3, we will have to introduce an additional boundary condition for the offshore boundary. This time instead of choosing a boundary condition that is compatible with an bay of infinite length, we choose to model a sloping bay of finite length with a wall located at some offshore distance x_L . Our choice of bathymetry is to facilitate the development of a spectral solution. It is notable that by placing the wall far away from the shore, bays of arbitrary length can be modeled. It also worth noting that our work in this chapter is similar to the work done by Baran [Bar11], Kanoglu [KS06a] and Garayshin [Gar13]. In particular Baran [Bar11] found a spectral solution for the case of parabolic bays, Kanoglu [KS06a] found a Green's function solution in parabolic bays that is valid for any initial velocity and Garayshin [Gar13] found a solution to the spectral problem in U and V shaped bays of infinite length.

To test our method we will compare our spectral solution to the analytic solution discussed in Chapter 2.3. The convergence of the spectral solution will be quantified by the error in the approximation of the initial condition. Furthermore the metric that will be used to validate our method will be the maximum relative error between our spectral solution and the analytic solution on domain away from the wall. Similar to Chapter 3, this method is shown to be both extremely fast and accurate.

4.1 Development of an IVBP

Recall that a spectral solution for a partial differential equation (PDE) is a series solution is a series solution where the elements of the series are separable solutions to the PDE.

Furthermore recall that the spatial functions in our transform are found by solving the Sturm-Liouville problem for the spatial operator of the PDE. We thus develop a Sturm-Liouville problem for a constantly sloping U and V shaped bay of finite length. The reader is referred to pages 41-88 of Al-Gwaiz's excellent book for a review of the basics results of Sturm-Liouville theory [AG07]. We first note that the spatial operator of (2.5) is not formally self-adjoint. Using the integrating factor $e^{\int W(\sigma)d\sigma} = \sigma^{1+2/m}$. Equation (2.5) is thus rewritten in self adjoint form as

$$\Phi_{\lambda\lambda} = \frac{1}{\sigma^{1+2/m}} \left(\frac{\partial}{\partial\sigma} (\sigma^{1+2/m}\Phi_{\sigma}) \right). \quad (4.1)$$

The first boundary condition (2.8) is already in an appropriate form for Sturm-Liouville theory, so we simply take

$$\Phi_{\sigma}(0, \lambda) = 0 \quad (4.2)$$

to be our shore boundary condition.

Now at the offshore boundary x_L , we assume that there is a physical wall. To simulate this, we impose $u(x_L, t) = 0$. This condition simulates a reflection of outgoing waves back towards the shore. For a discussion of the this wall condition the interested reader is referred to [KS06a, AB07, Bar11]. For our purposes this condition is slightly problematic and in fact can be a limiting factor for what waves can be modeled via this method. Sturm-Liouville theory requires $\sigma_L(x_L, t)$ must be fixed but the transformation from nonphysical to physical coordinate systems (2.6) condition gives us that $x_L = 1/\alpha(\eta(\sigma_L, \lambda) - H(x_L))$. Therefore if $\eta(\sigma_L, \lambda)$ is not constant at the offshore boundary, then either σ_L or x_L must change in respect to time. To solve this potential issue note that when $\eta(\sigma_L, \lambda) \ll H(\sigma_L)$ for all relevant λ then $x_L \approx \text{constant}$ for constant σ_L . Physically this is the assumption that the wave height at the wall is small when compared to the depth of the unperturbed water height at the wall. Under this assumption, we compute an initial σ_L from (2.2) and allow x_L to change freely within a small range of values. In general the acceptable variance of x_L will be dependent on the application in question but for benchmarking numerical models the change in x_L should be less than the spatial grid size used in the numerical model being benchmarked. Under the assumption that σ_L and x_L are both fixed, (2.6) allows our boundary condition to be written as

$$\Phi_{\sigma}(\sigma_L, \lambda) = 0. \quad (4.3)$$

We now note that (4.2)-(4.3) are both self-adjoint conditions for a Sturm-Liouville problem.

With boundary conditions worked out, we translate the initial conditions (2.7) into appropriate initial conditions for Sturm-Liouville theory. For convince we would like to have initial conditions for $\Phi(\sigma, 0)$ and $\Phi_\lambda(\sigma, 0)$. We thus take the condition for $\Phi_\lambda(\sigma, 0)$ as given and integrate the condition for $\Phi_\sigma(\sigma, 0)$. Our initial conditions are thus given by

$$\Phi(\sigma, 0) = \frac{m}{m+1} \int_0^\sigma u_0(x(\sigma', 0)) \sigma' d\sigma', \quad \Phi_\lambda(\sigma, 0) = 2g\eta_0(x(\sigma, 0)) + u_0^2(x(\sigma, 0)), \quad (4.4)$$

4.2 Spectral Solution to the IVBP

We now develop a spectral solution to the IVBP given by (4.1) with the boundary conditions (4.2)-(4.3) and the initial conditions (4.4). To find a spectral solution we first need to find the eigenfunctions and eigenvalues to the eigenvalue problem

$$\frac{1}{\sigma^{1+2/m}} \left(\frac{\partial}{\partial \sigma} (\sigma^{1+2/m} f_\sigma) \right) = -v^2 f \quad f'(0) = 0, \quad f'(\sigma_L) = 0. \quad (4.5)$$

The choice of negative separation constant, $-v^2$, is to ensure that our eigenfunctions are oscillatory and not exponentially decreasing. To solve (4.5) we employ a transformation used by Baran [Bar11] and Garayshin [Gar13]. We first expand (4.5) and multiply by $\sigma^{1/m+1}$. We then introduce the parameter $\gamma = 1/m$ and assume that $f = \sigma^{-\gamma} g(\sigma)$ where $g(\sigma)$ is an arbitrary function. Finally we make the change of variables $\sigma = t/v$. Under this transformation (4.5) becomes the Bessel equation

$$t^2 g_{tt} + t g_t + (t^2 - \beta^2) g = 0$$

with the boundary conditions

$$g(0) = 0 \text{ and } \sigma_L g'(\sigma_L) - \gamma g(\sigma_L) = 0. \quad (4.6)$$

Note that

$$g(\sigma) = C_1 J_\gamma(t) + C_2 Y_\gamma(t),$$

is the general solution to Bessel's equation where $J_\gamma(t)$ and $Y_\gamma(t)$ are the Bessel function of the first and second kinds respectively [AWH12]. To applying the boundary conditions (4.6) we note that $J_\gamma(0) = 0$ for all γ and that $Y_\gamma(0)$ is unbounded for each γ [AWH12]. Using these facts, the boundary condition at 0 forces $C_2 = 0$. To avoid a trivial solution $C_1 \neq 0$ and so v must be a positive zero of the equation

$$\sigma_L J'_\gamma(\sigma_L v) - \gamma J_\gamma(\sigma_L v) = 0. \quad (4.7)$$

Using the transform from f to g , it follows that the set of functions

$\{f_n(\sigma)\} = \left\{ \frac{J_\gamma(\sigma v_n)}{\sigma^\gamma} \middle| \text{where } v_n \text{ solves (4.7)} \right\}$ is the solution to the eigenvalue problem (4.5). According to Sturm-Liouville theory because the operator $1/\sigma^{1+2/m} \left(\frac{\partial}{\partial \sigma} (\sigma^{1+2/m} X_\sigma) \right)$ is a self-adjoint operator with weight function σ^{1+2m} it follows that

$$\int_0^{\sigma_L} \frac{J_\gamma(\sigma v_i)}{\sigma^\gamma} \frac{J_\gamma(\sigma v_k)}{\sigma^\gamma} \sigma^{1+2\gamma} d\sigma = A_i \delta_{ik} \quad (4.8)$$

where δ_{ik} is the Dirac delta function and $A_i = \int_0^{\sigma_L} J_\gamma^2(\sigma v_i) \sigma d\sigma$. Equation (4.8) is an orthogonality condition for our eigenfunctions. Upon solving the temporal equation ($\Phi_{\lambda\lambda} = -v_n^2 \Phi$) the spectral solution to (4.1) with (4.2)-(4.3) is

$$\Phi(\sigma, \lambda) = \sum_{n=1}^{\infty} \left(\frac{J_\gamma(v_n \sigma)}{\sigma^\gamma} (E_n \sin(v_n \lambda) + F_n \cos(v_n \lambda)) \right). \quad (4.9)$$

Applying the initial conditions (4.4) and multiplying by $(J_\gamma(v_i \sigma)/\sigma^\gamma) \sigma^{1+2\gamma}$ yields

$$\sum_{n=1}^{\infty} F_n \frac{J_\gamma(v_n \sigma)}{\sigma^\gamma} \frac{J_\gamma(v_i \sigma)}{\sigma^\gamma} \sigma^{1+2\gamma} = \frac{m}{m+1} J_\gamma(v_i \sigma) \sigma^{2+\gamma} \int_0^\sigma u_0(x(\sigma', 0)) \sigma' d\sigma'$$

and

$$\sum_{n=1}^{\infty} v_n E_n \frac{J_\gamma(v_n \sigma)}{\sigma^\gamma} \frac{J_\gamma(v_i \sigma)}{\sigma^\gamma} \sigma^{1+2\gamma} = (2g\eta_0(x(\sigma, 0)) + u_0^2(x(\sigma, 0))) J_\gamma(v_i \sigma) \sigma^{1+\gamma}.$$

We now integrate along our domain and apply the orthogonality condition (4.8) to see that

$$F_n = \frac{m}{(m+1)A_n} \int_0^{\sigma_L} \left(J_\gamma(v_i \sigma) \sigma^{1+\gamma} \int_0^\sigma u_0(x(\sigma', 0)) \sigma' d\sigma' \right) d\sigma \quad (4.10)$$

and

$$E_n = \frac{1}{v_n A_n} \int_0^{\sigma_L} ((2g\eta_0(x(\sigma, 0)) + u_0^2(x(\sigma, 0))) J_\gamma(v_i \sigma) \sigma^{1+\gamma}) d\sigma. \quad (4.11)$$

Putting our work together, the series (4.9) where v_n solves (4.7), F_n is given by (4.10) and E_n is given by (4.11), is a solution to (4.1) with boundary conditions (4.2)-(4.3) and initial conditions (4.4).

4.3 Numerical Implementation of the Spectral Solution

We now demonstrate how to implement the spectral solution in Matlab [MAT11]. The primary difficulties in computing our solution are accurately computing the eigenvalues and accurately computing all the integrals that are involved. Note that our eigenvalues can be put in order from smallest to largest. Furthermore, as the eigenvalue is related to the frequency of the corresponding eigenfunction and as high frequency eigenfunctions are not good approximations to long waves (thus will have small coefficients), it is natural to order our eigenvalues from smallest to largest. This poses an issue when numerically computing the spectrum. Namely, since the earlier eigenfunctions better approximate our initial condition we must ensure that the eigenvalues are in order from smallest to largest without missing eigenvalues. Furthermore the accuracy of the eigenvalues are of keen interest since it is the eigenvalues that define the family of functions used in the construction of our solution. Thus, error in the eigenvalues will introduce error everywhere. One more critical aspect for the numerical implementation of our solution is determining what criteria to use to truncate our solution to a finite sum. One natural metric for the convergence of our method is how well the solution approximates the initial condition. This is the metric we will use. Finally we must also check that all of the integrals we compute are sufficiently accurate.

Here is the algorithm we developed to compute the runup utilizing the spectral solution:

1. Using the information from the physical problem compute σ_L and $\sigma(x)$ via the method in Chapter 2.4.
2. For some starting number of eigenvalues N , compute the first N eigenvalues, v_n , by finding the first N positive roots of (4.7). We accomplish this by utilizing the open-

source software Chebfun. Chebfun is a good choice as it uses a combination of the recursive bisection method and the Colleague Matrix (a Chebyshev analogue of the Companion Matrix) to find all roots within a given interval [Tre13].

3. Compute E_n and F_n from (4.11) and (4.10) and thus the potential $\Phi(\sigma, \lambda)$ via (4.9).
4. Find the corresponding physical solution via the method outlined in Chapter 2.4.
5. Check for the error in the approximation of the initial condition. If the error is not sufficiently small repeat steps 2-4 with a larger N .
6. Once sufficient convergence is found the resulting (x, t) points will not be on an even grid. We thus interpolate our solution onto an even grid [KS98, HNPR15].

4.4 Verification and Validation of the Spectral Method

We now test how well our solution works on the same sample runup problem in Chapter 3.2.1. In particular we compare our method to the analytic solution discussed in Chapter 2.3 and then give a numerical demonstration of the effect of m on the maximum runup. Note that both the analytic solution and the numeric algorithm in Chapter 3 are for bays of infinite length. Thus to be able to compare our spectral solution to those solutions we must make sure that there is no interference from the boundary. To this effect, we will only compare the models within space time locations where the wave has not reflected back from the wall.

4.4.1 Verification in a Parabolic Bay

To be consistent we will use the same wave profile and bay that was used to verify the model discussed in Chapter 3. Recall that we used the initial profile $\eta(\sigma, 0) = \frac{2A(\sigma - \sigma_0)}{2gp^2} e^{-(\sigma - \sigma_0)^2/p^2}$ in a constantly sloping parabolic bay ($\alpha = .1$) where the constants were given by $A = 0.5$, $p = 1.5$ and $\sigma_0 = 15$ (see Figure 1.1). Also recall that the values of runup and rundown for this problem are $R_u \approx 0.1322$ and $R_d \approx -0.2963$ respectively.

Before we can talk about the runup characteristics of the spectral solution, we must examine the movement of the physical wall. Since we are comparing our spectral solution to

the analytic solution given in Chapter 2.3, we place the wall boundary far enough away from the shore such that the solutions are comparable. We thus put the initial wall 2666 units away from the shore. The maximum deviation from this length was .04 units. This should be well within the range one would need for many applications.

The spectral method gives a maximum runup of .1318 and a minimum rundown of $-.2951$. The relative error at maximum runup is 0.30% and the relative error at the minimum rundown is 0.40%. This is better than the semianalytic method used in Chapter 3 as the relative errors were 0.35% and 0.65% respectively. Figure 4.1 shows the error in our initial condition as well as the values of the first 50 coefficients in our expansion. In Figure 4.2 we show several plots comparing the spectral solution to the analytic solution found in Chapter 2.3. In the top two plots the wave can be seen bouncing off of the wall in the spectral model but passing through in the analytic solution. The black lines in the top two plots represent an area where the two solutions can be compared. Furthermore, the bottom plot shows the error comparison near the shore in terms of relative error.

These results suggest that this method may be more accurate than our spectral method may be more accurate than the semianalytic method developed in Chapter 3. Furthermore the computational time required for this test of the spectral method is extremely negligible (20-30 seconds).

4.5 Runup in U vs. V Shaped Bays

As an application of our method we run a numerical experiment to examine the wave runup in U vs. V shaped bays. In particular we choose the initial profile $\eta(\sigma, 0) = \frac{2A(\sigma-\sigma_0)}{2gp^2} e^{-(\sigma-\sigma_0)^2/p^2}$ in a constantly sloping bay with cross-section of the form $f(y) = |y|^m$ ($\alpha = .1$) where the constants were given by $A = 0.5$, $p = 1.5$ and $\sigma_0 = 15$ (see Figure 1.1) and then examine how the runup changes when m is varied. Figure 4.3 shows the results of this experiment. For this particular bay slope and initial condition, the statement that wave runup in V shaped bays is larger than the runup in U shaped bays is verified.

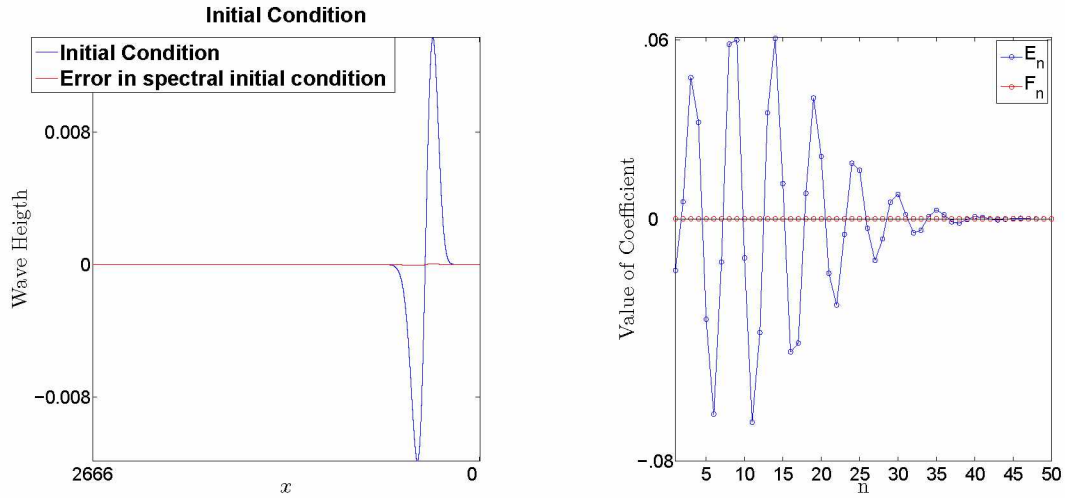


Figure 4.1: Left: the accuracy in the approximation of the initial condition using our spectral method, Right: The coefficients in the spectral expansion corresponding to the initial condition to the left.

4.6 Conclusions

An initial value boundary problem is developed for U and V shaped bays of finite length and a spectral method is applied. The spectral method presented here is yet another example of how the generalized Carrier-Greenspan transformation can be used as a numerical tool. Our method computes extremely fast taking only 30 to 40 seconds as compared to two days in FUNWAVE.

For runup in infinite bays the limitation at the offshore wall is only an apparent limitation. By extending the length of the finite bay, wave runup in infinite bays can be simulated. To this affect, as $\sigma_L \rightarrow \infty$ our solution approximates the solution found by Garayshin [Gar13]. For wave runup in wave tanks of finite length the limitation at the offshore wall may pose issues depending on the application.

Finally as an application of our method we have provided evidence that runup in V shaped bays is greater than runup in U shaped bays with all other factors held constant.

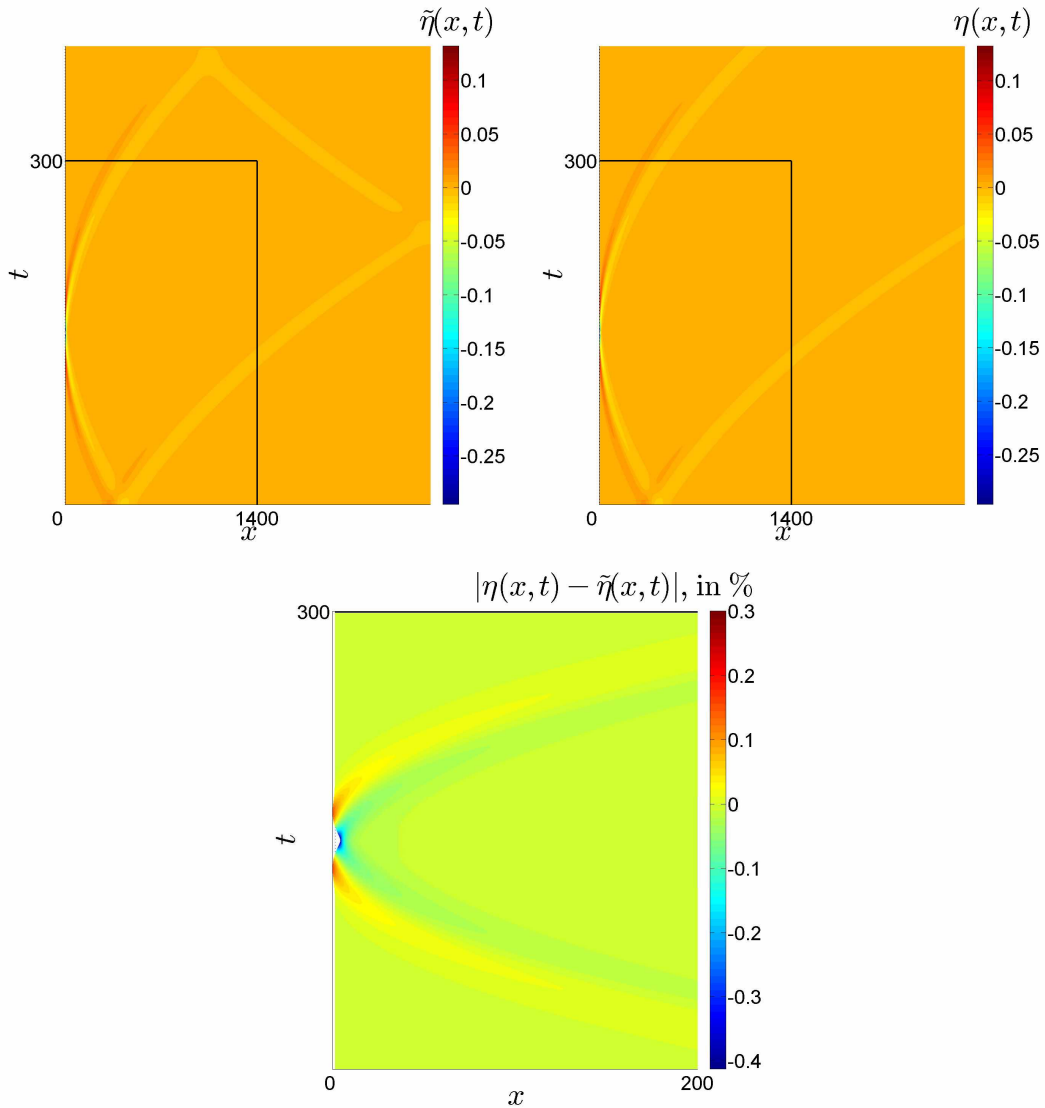


Figure 4.2: Top Left: the wave dynamics as computed by the spectral method. The black lines show a domain where our spectral solution can be compared against the analytic one. Top Right: analytic solution to be compared to our spectral method. Bottom: The relative error in terms of the maximum runup. The maximum errors occur at the runup (0.3%) and rundown (0.4%).

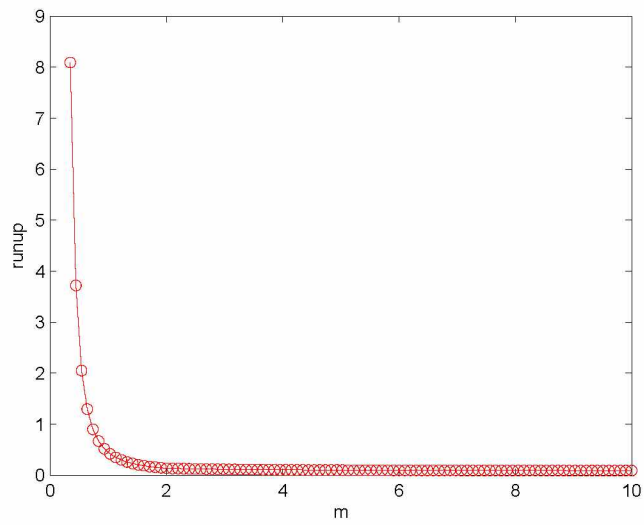


Figure 4.3: The effect of m on runup. Recall that bays with $0 < m \leq 1$ are V shaped bays and bays with $m > 1$ are the U shaped bays. This plot shows that for the initial condition, the runup in V shaped bays is significantly larger than the runup in U shaped bays.

Chapter 5

Conclusions

In this study, we have demonstrated the usefulness of the generalized Carrier-Greenspan transform for numerically computing long wave runup characteristics by developing two numerical implementations for the generalized Carrier-Greenspan transform – a finite difference method and a spectral solution. The finite difference method is valid for any constantly sloping bays of infinite length with arbitrary cross sections where as the spectral method is valid for any constantly sloping bays of finite length with U or V shaped cross sections.

The accuracy of these methods were tested via a comparison to an known analytic with positive results. A comparison to a 3D numerical solver was made for the finite difference method and it was shown that our method predicted runup/rundown values close to what FUNWAVE gave. This shows that our methods can be used to compute approximations to real world runup. Furthermore our methods give a significant improvement in runtime over FUNWAVE with the finite difference method taking 2 minutes, the spectral method taking 30-40 seconds and FUNWAVE taking 2 days to run.

Because of the limited resources required to compute the runup and rundown via our methods, these methods could be used to compute real time runup maps for areas that currently do not have emergency models in place. This greatly extends the range of locations that can develop inundation maps for evacuation plans.

Our methods can also be used to study the general effects a bathymetry has on the wave runup. We demonstrated this by examining the effect of the power of a U or V shaped bay on the runup. The results of this numerical study agree with recent studies on local runup in the case of the 2011 Japan tsunami. The ability to quickly examine the effect of the bathymetry on the wave runup could lead to a deeper understanding of how to defend

against a tsunami. In particular for high population locations that are at a high tsunami risk, coastal engineering could be done to change some of the local features of a bay and thus lower the maximum wave runup.

The ability to quickly run numerical experiments has the potential to find new wave runup phenomena with less work on the part of the researcher. For example one could algorithmically choose the parameters of a bay and an initial wave profile, let the algorithm run, and then search the results for interesting wave behavior.

This research leads to several open problems. We conclude with a list of interesting open problems: Can these methods be generalized to piecewise sloping bays as in [Syn87]? Can we generalize our methods to work for nonzero initial velocity as in [KS06a]? How does the finite difference method work for bays that are shaped like a W ? What class of initial conditions can be decomposed into our spectral series?

References

- [AB07] M. Antuono and M. Brocchini. The boundary value problem for the nonlinear shallow water equations. *Studies in Applied Mathematics*, 119:73–93, 2007.
- [AG07] Mohammed Al-Gwaiz. *Sturm-Liouville Theory and its Applications*. Springer, 2007.
- [AS65] Milton Abramowitz and Irene Stegun. "Chapter 17", *Handbook of Mathematical Functions with Formulas, Graphs, and Mathematical Tables*. Dover, 1965.
- [AWH12] George Brown Arfken, Hans-Jurgen Weber, and Frank E. Harris. *Mathematical Methods for Physicists: A Comprehensive Guide*. Academic Press, 2012.
- [Bar11] A. Baran. *Analytical Solutions of Shallow-Water Wave Equations*. PhD thesis, Middle East Technical University, 2011.
- [BDN⁺11] H.M. Benz, R.L. Dart, A. Villase Nor, G.P. Hayes, A.C. Tarr, K.P. Furlong, and S. Rhea. Seismicity of the earth 1900 2010 aleutian arc and vicinity. Open-file report 2010 083-b, U.S. Geological Survey, 2011. scale 1:5,000,000.
- [BR09] E.N. Bernard and A.R. Robinson. Chapter 1, introduction: Emergent findings and new directions in tsunami science. *Harvard University Press.*, 2009.
- [CFL28] R. Courant, K.O. Friedrichs, and H. Lewy. Über die partiellen differenzgleichungen der mathematischen physik. *Mathematische Annalen*, 100:32–74, 1928.
- [CG57] George Carrier and H.P. Greenspan. Water waves of finite amplitude on a sloping beach. *Journal of Fluid Mechanics*, 01:97–109, 1957.
- [CWY02] George Carrier, Tai Tei Wu, and Harry Yeh. Tsunami run-up and draw-down in a plane beach. *Journal of Fluid Mechanics*, 475:79–99, 2003.

- [Did13] I. Didenkulova. Tsunami runup in narrow bays: the case of Samoa 2009 tsunami. *Natural Hazards*, Vol. 65 (3):1629–1636, 2013.
- [DP11a] I. Didenkulova and E. Pelinovsky. Non-linear wave evolution and run-up in an inclined channel of a parabolic cross-section. *Physics of Fluids*, 23:086602, 2011.
- [DP11b] I. Didenkulova and E. Pelinovsky. Runup of tsunami waves in U-shaped bays. *Pure and Applied Geophysics*, 168:1239–1249, 2011.
- [DW08] P.K. Dunbar and C.S. Weaver. U.S. states and territories. national tsunami hazard assessment: Historical record and sources for waves. Technical report, NOAA and USGS, 2008. 59 pp.
- [Ewi11] L. Ewing. The Tohoku tsunami of March 11, 2011: A preliminary report on effects to the California coast and planning implications. Technical report, California Coastal Commission, 2011. 40 pp.
- [FBS⁺11] H.M. Fritz, J.C. Borrero, C.E. Synolakis, E.A. Okal, R. Weiss, P.J. Lynett, V.V. Titov, S. Foteinis, B.E. Jaffe, P.L.-F. Liu, and I.-C. Chan. Insights on the 2009 south pacific tsunami in samoa and tonga from field surveys and numerical simulations. *Earth Science Review*, 107:66–75, 2011. doi:10.1016/j.earscirev.2011.03.004.
- [Fle91] C.A.J. Fletcher. *Computational Techniques for Fluid Dynamics 1*. Springer-Verlag, 1991. 401 pp.
- [FPC⁺11] H.M. Fritz, C.M. Petroff, P. Catalan, R. Cienfuegos, P. Winckler, N. Kalligeris, R. Weiss, S.E. Barrientos, G. Meneses, C. Valderas-Bermejo, Ebeling, C., A. Papadopoulos, M. Contreras, Dominguez J.C. Almar, R., and C.E. Synolakis. Field survey of the 27 february 2010 chile tsunami. *Pure Appl. Geophys*, 168(11):1989–2010, 2011. doi:10.1007/s00024-011-0283-5.
- [Gar13] V. Garayshin. Tsunami runup in U and V shaped bays. Master’s thesis, University of Alaska Fairbanks, 2013.

- [GMO97] V.K. Gusiakov, A.G. Marchuk, and A.V. Osipova. *Perspectives on Tsunami Hazard Reduction*, chapter Expert tsunami database for the Pacific: motivation, design and proof-of-concept demonstration, pages 21–43. Kluwer Academic Publishers, 1997. Available at http://tsun.sccc.ru/tsulab/On_line_Cat.htm.
- [GST01] S. Gottlieb, C.-W. Shu, and E. Tadmor. Strong stability-preserving high-order time discretization methods. *SIAM Review*, 43(1):89–112, 2001.
- [HNPR15] M.W. Harris, D.J. Nicolsky, E.N. Pelinovsky, and A.V. Rybkin. Runup of nonlinear long waves in trapezoidal bays: 1-D analytical theory and 2-D numerical computations. *Pure and Applied Geophysics*, pages 1–15, 2015.
- [Kan04] U. Kanoglu. Nonlinear evolution and runup and rundown of long waves over a sloping beach. *Journal of Fluid Mechanics*, 513:363–372, 2004.
- [Kif12] D. Kiffer. We all survived the great tsunami alert of 2012! SitNews: Column, October 30 2012. http://www.sitnews.us/DaveKiffer/103012_kiffer.html.
- [KKP⁺13] D.C. Kim, K.O. Kim, E. Pelinovsky, I. Didenkulova, and B.H. Choi. Three-dimensional tsunami runup simulation at the Koborinai port, Sanriku coast, Japan. *Journal of Coastal Research*, vol.65:266–271, 2013.
- [KS98] U. Kanoglu and C. E. Synolakis. Long wave runup on piecewise linear topographies. *Journal of Fluid Mechanics*, 1-28:374, 1998.
- [KS06a] U. Kanoglu and C. Synolakis. Initial value problem solution of nonlinear shallow water-wave equations. *Physical Review Letters*, 2006.
- [KS06b] U. Kanoglu and C. E. Synolakis. The initial value problem solution of nonlinear shallow-water wave equations. *Physical Review Letters*, 97:148501, 2006.
- [LST⁺13] H. Liu, T. Shimozone, T. Takagawa, A. Okayasu, H.M. Fritz, S. Sato, and Y. Tajima. The 11 march 2011 tohoku tsunami survey in rikuzentakata and comparison with historical events. *Pure Appl. Geophys*, 170(6-8):1033–1046, 2013. doi:10.1007/s00024-012-0496-2.

- [MAT11] MATLAB. *version 7.13.0.564 (R2011b)*. The MathWorks Inc., Natick, Massachusetts, 2011.
- [MP01] S.R. Massel and E.N. Pelinovsky. Run-up of dispersive and breaking waves on beaches. *Oceanologia (Poland)*, 43:61–97, 2001.
- [Nat14] National Police Agency of Japan. Damage situation and police countermeasures associated with 2011tohoku district - off the pacific ocean earthquake. *National Police Agency of Japan*, 2014.
- [NCD11] Dick K. Nanto, William H. Cooper, and J. Michael Donnelly. Japans 2011 earthquake and tsunami: Economic effects and implications for the united states. *Congressional Research Service*, 2011.
- [NGD13] NGDC. National Geophysical Data Center / (NGDC/WDS) global historical tsunami database. Technical report, NGDC, Boulder, CO, USA, 2013. Available at http://www.ngdc.noaa.gov/hazard/tsu_db.shtml.
- [Pel95] E. Pelinovsky. Nonlinear hyperbolic equations and run-up of huge sea waves. *Applicable Analysis*, 57:63–84, 1995.
- [PM92] E. Pelinovsky and R. Mazova. Exact analytical solutions of nonlinear problems of tsunami wave run-up on slopes with different profiles. *Natural Hazards*, 6:227–249, 1992.
- [PT94] E.N. Pelinovsky and E.N. Troshina. Propagation of long waves in straits. *Phys. Oceanography*, 5:43–48, 1994.
- [RLK07] N.A. Ruppert, J.M. Lees, and N.P. Kozyreva. *Volcanism and Subduction: The Kamchatka Region*, volume 172 of *Geophysical Monograph Series*, chapter Seismicity, Earthquakes and Structure Along the Alaska-Aleutian and Kamchatka-Kurile Subduction Zones: A Review, pages 129–144. American Geophysical Union, Washington, D.C., 2007.
- [RPD14] A.V. Rybkin, E. Pelinovsky, and I. Didenkulova. Non-linear wave run-up in bays of arbitrary cross-section:generalization of the Carrier-Greenspan approach. *Journal of Fluid Mechanics*, 748:416–432, 2014.

- [SB06] C.E. Synolakis and E.N. Bernard. Tsunami science before and beyond Boxing Day 2004. *Philosophical Transactions of the Royal Society A*, 364:2231–2265, 2006.
- [SBT⁺08] CE Synolakis, EN Bernard, VV Titov, U Kanoglu, and F Gonzalez. Validation and verification of tsunami numerical models. *Pure Applied Geophysics*, 165:2197–2228, 2008.
- [SCP⁺14] T. Shimozono, H. Cui, J.D. Pietrzak, H.M. Fritz, A. Okayasu, and A.J Hooper. Short wave amplification and extreme runup by the 2011 tohoku tsunami. *Pure Appl. Geophys*, 2014. doi: 10.1007/s00024-014-0803-1 (online first, in press).
- [Shu73] N. Shuto. Shoaling and deformation of nonlinear long waves. *Coastal Eng. Japan*, 16:1–12, 1973.
- [SKH⁺12] F. Shi, J.T. Kirby, J.C. Harris, J.D. Geiman, and S.T. Grilli. A high-order adaptive time-stepping tvd solver for boussinesq modeling of breaking waves and coastal inundation. *Ocean Modeling*, 43-44:36–51, 2012.
- [Spi76] L. O. Spielfogel. Single-wave run-up on sloping beaches. *J. Fluid Mech.*, 74:685 – 694, 1976.
- [SSO⁺12] T. Shimozono, S. Sato, A. Okayasu, Y. Tajima, H.M. Fritz, H. Liu, and T. Takagawa. Propagation and inundation characteristics of the 2011 Tohoku Tsunami on the Central Sanriku Coast. *Coastal Eng. J*, pages 54(1):1250004,, 2012. doi:10.1142/S0578563412500040.
- [Sto57] J.J. Stoker. *Water waves: The Mathematical Theory with Applications*. Interscience Publishers, 1957.
- [Syn87] C.E. Synolakis. The runup of solitary waves. *Journal of Fluid Mechanics*, 185:523–545, 1987.
- [Syn91] C.E. Synolakis. Tsunami runup on steep slopes: how good linear theory really is? *Natural Hazards*, 4:221–234, 1991.

- [TKMS12] B. Tehranirad, J.T. Kirby, G. Ma, and F. Shi. Tsunami benchmark results for nonhydrostatic wave model NHWAVE (Version 1.1). Research report no. cacr-12-03, Center for Applied Coastal Research, University of Delaware, Newark, 2012.
- [Tor09] E.F. Toro. *Riemann solvers and numerical methods for fluid dynamics: a practical introduction*. Springer, New York, 2009.
- [Tre13] Lloyd Trefethen. *Approximation theory and approximation practice*, 2013.
- [TS94] S. Tadepalli and C. Synolakis. The runup of n-waves. *Roy. Soc. London*, A445:99–112, 1994.
- [TSK⁺12] B. Tehranirad, F. Shi, J.T. Kirby, J.C. Harris, and S. Grilli. Tsunami benchmark results for fully nonlinear boussinesq wave model funwavetvd, version 1.0. In *Proceedings and Results of the 2011 NTHMP Model Benchmarking Workshop*, page p. fix it, Boulder, CO, 2012. U.S. Department of Commerce/NOAA/NTHMP, NOAA Special Report. (available at <http://nthmp.tsunami.gov>).
- [TT05] S. Tinti and R. Tonini. Analytical evolution of tsunamis of seismic origin on a constant slope ocean. *J. Fluid Mech.*, 2005.
- [TTC09] L. Tang, V.V. Titov, and C.D. Chamberlin. Development, testing, and applications of site-specific tsunami inundation models for real-time forecasting. *J. Geophys. Res.*, 114:C12025, 2009. doi:10.1029/2009JC005476.
- [WAB⁺13] R.I. Wilson, A.R. Admire, J.C. Borrero, L.A. Dengler, M.R. Legg, P. Lynett, T.P. McCrink, K.M. Miller, A. Ritchie, K. Sterling, and P.M. Whitmore. Observations and impacts from the 2010 Chilean and 2011 Japanese tsunamis in California (USA). *Pure and Applied Geophysics*, 170:1127–1147, 2013.
- [WMew] R.I. Wilson and K.M. Miller. Tsunami emergency response playbooks. Special report, California Geological Survey, in review.
- [ZPGO06] Narcisse Zahibo, Efim Pelinovsky, Vladimir Golinko, and Nataly Osipenko. Tsunami wave runup on coasts of narrow bays. *International Journal of Fluid Mechanics Research* 33.1, 2006.